APPLICATION OF COSMIC-RAY PROBE FOR THE DETECTION OF FREEZING-THAWING PROCESS OVER TIBETAN PLATEAU

JINBANG PENG
February, 2017

SUPERVISORS:
Dr. Y. Zeng
Prof.Dr. Z. Su

ADVISOR:
Dr. L. Yu

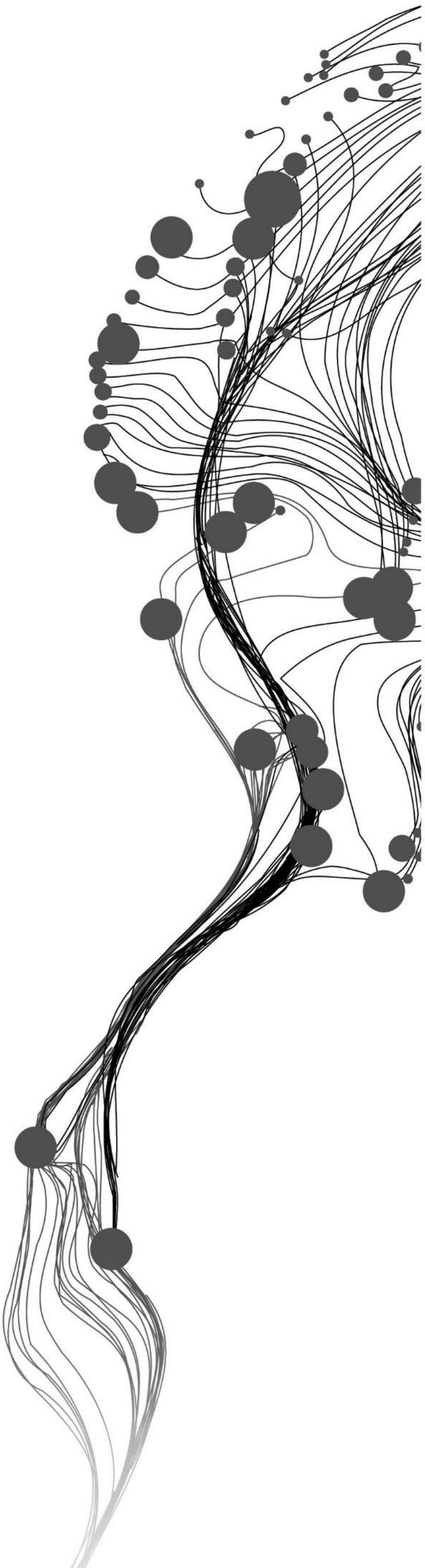

APPLICATION OF COSMIC-RAY PROBE FOR THE DETECTION OF FREEZING-THAWING PROCESS OVER TIBETAN PLATEAU

JINBANG PENG
Enschede, the Netherlands, February, 2017

Thesis submitted to the Faculty of Geo-Information Science and Earth Observation of the University of Twente in partial fulfilment of the requirements for the degree of Master of Science in Geo-information Science and Earth Observation.
Specialization: Water resources and Environment Management

SUPERVISORS:
Dr. Y. Zeng
Prof.Dr. Z. Su

ADVISOR:
Dr. L. Yu

THESIS ASSESSMENT BOARD:
Dr.Ir. C.M.M. Mannaerts (Chair)
Dr. V Bense (External examiner, Wageningen University & Research)

ABSTRACT

The cosmic-ray neutron probe (CRP) is a newly developed machine, which can detecting the soil water content in intermediate scale. The application of this probe at Tibetan Plateau is not fully explored, where the ground is seasonally frozen. To study the applicability of CRP and detecting the Freezing/Thawing process on the Tibetan Plateau, a CRP was built in the study area Maqu country in Tibetan Plateau.

In this research, a field work was executed for the calibration of CRP. Then the validation of CRP was accomplished by comparing the CRP data with point measured soil water content data in two methods (N_0 method and COSMIC model method), both resulting in a well correlation. To develop a better understanding of the CRP in the study area, the footprint and measuring depth was derived. And to get a better application of the CRP data, an analysis about time window for smoothing the data from CRP was carried out, finding that 6 hours' time window is a suitable for smoothing the data in this study.

The detection of the freezing/thawing process started from the selection of model for simulating the correlation between soil temperature and liquid soil water content in the frozen ground. The newly adopted double exponential function was proved to be in high precise for describing the correlation, which provides a way for measuring the soil ice content by combining the CRP detected total soil water content and soil temperature correlated liquid soil water content. This result of soil ice content was compared with another approach for measuring the soil ice content which employed the CRP detected total soil water content and point measured liquid soil water content. And this comparison results revealed a high correlation between two kinds derived soil ice content.

Key words: CRP, soil water content, Tibetan Plateau, soil temperature, frozen ground, Freezing/ Thawing process

ACKNOWLEDGEMENTS

I would like to firstly address my gratitude to my dear parents and brother, who gave me the financial support to enjoy the wonderful life and study in the Netherlands.

I would like to sincerely express my respect and thanks my first supervisor Dr. Y. Zeng for giving me a chance to study this interesting topic and for his encouragement, guidance and patience through all the stage of this research. I would also like to extend my gratitude to my second supervisor Prof. Z. Su for his professional comments during the research. I would like to specially thank my advisor Dr. L. Yu who helped me unconditionally through all the research and always gave me the confidence to carry on the work when I was depressed in the research. My gratitude also goes to Dr. H. Zhao and Dr. X. Wang, for their generous helps in the field work. Without their helps, I absolutely cannot accomplish this research.

I would gratefully like to thank the nice person who always be around me, give the courage to my life and study in this foreign country.

I would also like to acknowledge all the people I met in this country, my friend, my teacher, my classmates or even the strange people, for you impressing me an unforgettable experience in this country.

TABLE OF CONTENTS

LIST OF FIGURES

LIST OF TABLES

LIST OF ACRONYMS

LSWC	Liquid soil water content
TSWC	Total soil water content
SWC	Soil water content
SIC	Soil ice content
ST	Soil temperature
SM	Soil moisture
FT	Freezing/thawing
COSMIC	COsmic-ray Soil Moisture Interaction Code
CRP	Cosmic-ray neutron probe
NMDB	Neutron Monitor Database

1. INTRODUCTION

1.1. Backgrouond

Although it occupied a very small part of the water on the planet, the water in soil is a significant parameter in the study of hydrology, meteorology, agriculture management and global climate change (Zhang et al., 2014). It plays a crucial role in the exchange of water and energy fluxes between the land surface and the atmosphere by controlling the partition of rainfall to subsoil drainage, surface runoff, or evaporation from the land surface (Wang & Qu, 2009; Su et al., 2011). As an indispensable part of vegetation's growth, soil water content affects the plant prosperity, especially in arid and semiarid ecosystem (Xiong, Johansson, Hughes, & Nilsson, 2003; D'Odorico, Caylor, Okin, & Scanlon, 2007).

Normally, the water in the soil is liquid, while ice is also possible to exist in the frozen ground. Over one-third of the global land area undergoes a seasonal transition between predominantly frozen and non-frozen conditions each year, with the land surface freeze/thaw (FT) process leading a significant control on hydrological and biospheric processes over northern land areas and at high elevation areas (Kim, Kimball, McDonald, & Glassy, 2011; Xu et al., 2016; Xu et al., 2016). To detect the unfrozen soil water content (USWC) and soil ice content (SIC) participated in the FT process is crucial for studying the climate and ecology of the frozen ground.

The FT measurement is realized mainly depending on two technologies: in-situ point measurement and satellite microwave sensing, with critical shortcomings for both. Point measurement is a widely used method to detect the soil moisture with high accuracy. However, The total soil water content (TSWC) is highly spatial heterogeneous and the FT process also updates according to the soil temperature (ST) (M. Zreda et al., 2012). To observe the FT process of unfrozen ground with in-situ point measurement, it is required to set observing network with dense measuring points and high temporal resolution, which is not realistic to do it at regional scale. As a result, it is uneconomic and impractical to take large scale and long term in-situ observation of soil moisture in frozen ground for environmental monitoring and other applications.

On the other hand, satellite remote sensing technique, depending on the surface permittivity which is predominantly influenced by the phase of water, can measure the FT process with the distinct advantage of globe coverage (Xu et al., 2016). However, this technique is impossible to avoid the limitations including the inability for detecting soil ice, a shallow vertical penetration depth of millimetres to centimetres, limited capability to penetrate vegetation or snow, sensitivity to surface roughness, discontinuous temporal coverage, and high cost of satellite missions (Marek Zreda, Desilets, Ferre, & Scott, 2008). Then the FT process derived from the remote sensing images is normally based on the threshold approach with uncertainties in the threshold value for various land surface scenarios(Kim, Kimball, Zhang, & McDonald, 2012; Podest, McDonald, & Kimball, 2014; Zhu et al., 2016). Furthermore, the spatial resolution of the satellite remote sensing approach is in kilometre scale, which means that the FT process result from this technology is not applicable in intermediate scale land surface and atmospheric models(M. Zreda et al., 2012).

In this study, the cosmic-ray method is adopted to measure the TSWC in frozen ground with both liquid soil water and soil ice existed. Although this method of neutron scattering determining soil water content was developed more than half century ago, its application was limited until recent years (Belcher, Cuykendall, & Sack, 1950; Gardner & Kirkham, 1952; Stone, Kirkham, & Read, 1955; Van Bavel, Underwood, &

Swanson, 1956). The cosmic-ray neutron probe (CRP) used in the cosmic-ray method is a tool designed to measure the fast neutrons generated in the collision between high energy neutrons and the nuclei(McHenry, 1963; Marek Zreda et al., 2008). Before diffused back into the air and detected by the CRP, the high energy neutrons are moderated by the atoms particularly by hydrogen atoms. Since the main source of hydrogen atoms is soil water, the high energy neutrons is inversely correlated with the TSWC, in both solid and liquid phases (Desilets, Zreda, & Ferré, 2010). The installed CRP with measuring depth of centimetres and horizontal scale of hectometres (Marek Zreda et al., 2008) can support the intermediate scale land surface models with TSWC update at high temporal frequency. Table 1-1 shows the comparison of the mentioned soil moisture measuring methods.

Table 1-1 Comparison of soil moisture measuring methods

Methods	Distinct Advantage	Disadvantage	Spatial Resolution
Point measurement	High accuracy	Soil ice undetectable	Meter scale
Satellite images retrieval	Wide coverage	Depth limited	Kilometre scale
CRP	Soil ice detectable	Costly	Hectometre scale

To simulate the FT process over the frozen ground, the cosmic-ray neutron counts measured by the CRP is combined with the ST for retrieving the liquid soil water content (LSWC) and SIC. Many experiment and in-situ measurement results reveal that the ST and LSWC are highly correlated, while the empirical models for simulating this correlation are various (Civan, 2000; Romanovsky & Osterkamp, 2000; Kurylyk & Watanabe, 2013; Wu, Lai, & Zhang, 2017). These solutions would be examined with the ST and LSWC data from the point measurement in the study area to pick out the optimal correlation model for area. Then this optimal model would be employed to illustrate the FT process in company with CRP.

1.2. Problem definition

The SIC in the frozen ground are hard to measure with normally used methods like point measurement and remote sensing measurement. The newly developed CRP soil moisture observation method is based on the detecting of hydrogen atoms in the soil, so it is possible to measure the TSWC in both solid and liquid phases at moderate scale over the frozen grounds (Desilets et al., 2010). This method has been applied to measuring the snow water equivalent under frozen precipitation and detecting the soil water content in different scenarios (forest, drip irrigated field, alpine meadow, farmland and mixed land use, etc), while the feasibility of CRP in the frozen ground over Tibetan plateau is still not fully examined (Bogena, Huisman, Baatz, Hendricks Franssen, & Vereecken, 2013; Trenton E. Franz et al., 2016; Xujun Han et al., 2016; Xujun Han, Jin, Li, & Wang, 2014; Heidbuchel, Guntner, & Blume, 2016; Kodama, Nakai, Kawasaki, & Wada, 1979; Zhu et al., 2016).

The high correlation between ST and LSWC in frozen ground is identified by many researchers, however the models for simulating this correlation are still controversial (Kurylyk & Watanabe, 2013; Musa, Ya, Anzhi, & Cunyang, 2016). The correlation between the ST and unfrozen soil water content depends on the soil properties, so different areas present distinct properties. Thus a calibration of this correlation models is indispensable in this study for the study area.

1.3. Research objectives

The main objective of this study is to detect the FT process over frozen ground by the combing the application of CRP and the optimal correlation model between ST and LSWC.

And the specific objectives of this study mainly include three aspects:

1) To calibrate the CRP measurement with both the N_0 method and COSMIC model at Tibetan Plateau;

2) To calibrate the correlation between ST and liquid soil water content at Tibetan Plateau;

3) To simulate the LSWC and SIC over Tibetan Plateau.

1.4. Research questions

To achieve the objectives defined above, the following questions are highlighted for this study sought to answer:

1) Is the cosmic-ray method still applicable in frozen ground with water in both liquid and solid phases?

2) How does the ST relate to the liquid soil water content at Tibetan Plateau?

3) How accurate is SIC derived from the neutron counts and ST?

1.5. Innovations

The innovations of this study include two aspects:

1) Different with its previous applications to measure the soil moisture or the snow water equivalent, the cosmic-ray soil moisture method is newly applied to observe the TSWC in both liquid and solid phases over the frozen ground, a not fully explored scenario.

2) The CRP is employed to detecting the FT process in company with the correlation between ST and LSWC in frozen ground.

1.6. Expected outputs

The expected outputs of this study are presented as follow:

1) The calibration result of CRP at Tibetan plateau;

2) The calibrated correlation between ST and unfrozen water at Tibetan Plateau;

3) The results of SIC and LSWC for illustrating FT process at Tibetan Plateau.

2. MATERIALS

2.1. Study area

The immense Tibetan Plateau with average elevation over 3000 m and total area more than 2.6 million km^2, acts as the biggest plateau in the mid-latitudes. It is located between latitudes from 26°00'12"N to 39°46'50"N, and longitudes from 73°18'52"E to 104°46'59"E, with majority of the ground frozen permanently or seasonally as shown in Figure 2-1. Since the frozen ground FT process is extremely sensitive to the climate change, this area plays a vital role for studying the climate of Asia, even the whole globe.

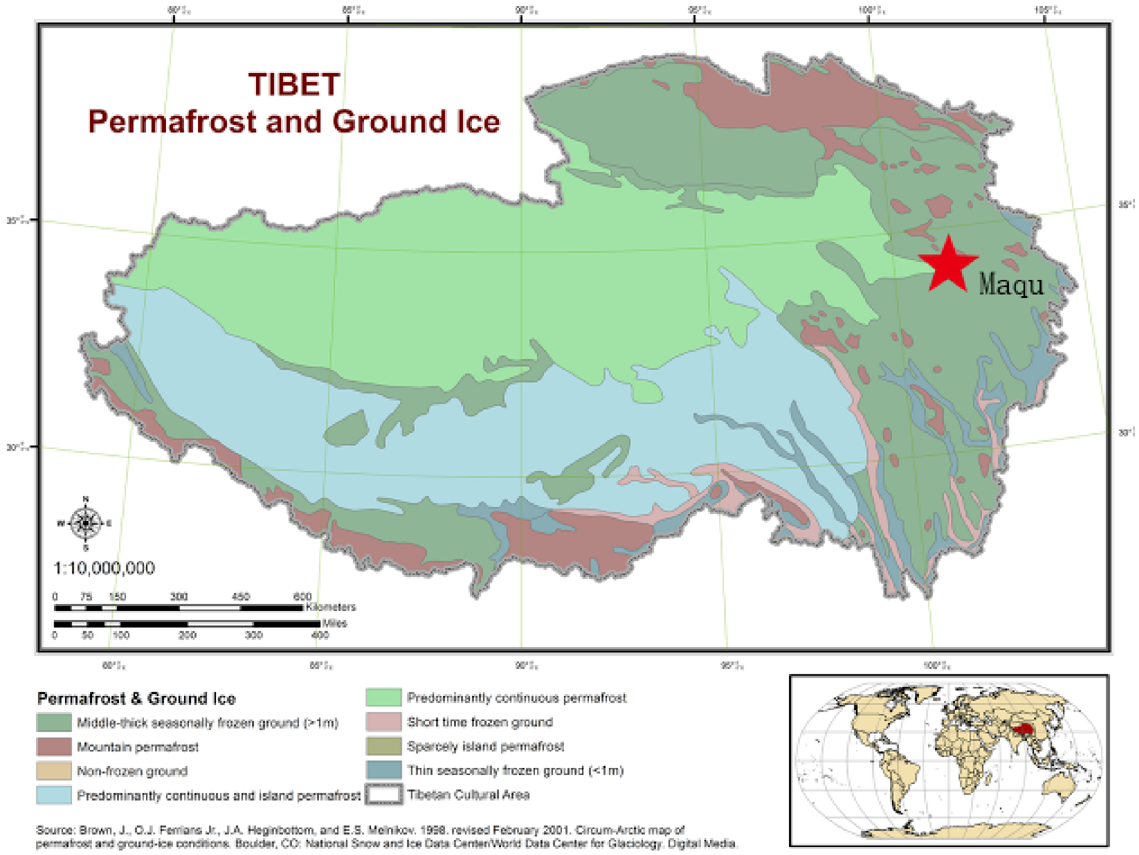

Figure 2-1 Distribution of frozen ground over Tibetan Plateau. The red star indicates the location of Maqu. (Source: http://tibet-edd.blogspot.nl/)

The study area Maqu is located in the north-eastern part of the Tibetan Plateau (Figure 2-1,Figure 2-2 and Table 2-1), with landscape dominated by alpine meadows. According to the Koeppen Classification System, the climate at this site is defined as wet and cold but seasonally distinct, with cold dry winters and cool rainy summers due to the monsoon (Su et al., 2011). The monthly average air temperature fluctuates between -10 °C and 12 °C, leading to the annual average air temperature about 1 °C (van der Velde et al., 2012). The precipitation is around 500–600 mm annually, with more than 70% falling during the monsoon season. The groundwater level is situated around 8.5–10.0 m below the surface (Zheng et al., 2015).

Table 2-1 Information about the CRP site

	Value	Unit
Site	Maqu	-
Latitude	33°54'59.55"	N
Longitude	102° 9'32.50"	E
Elevation (m)	3436	m
UTC Time Zone	8	-

The land cover within the footprint of CRP is typical alpine meadow grassland. The ground of this area is relatively flat with altitude deference less than one meter. The soil of this area belongs to silt loam, covered by grass about 10 cm on the surface for grazing by sheep and yaks as the sceneary shown in Figure 2-2 (Su et al., 2011).

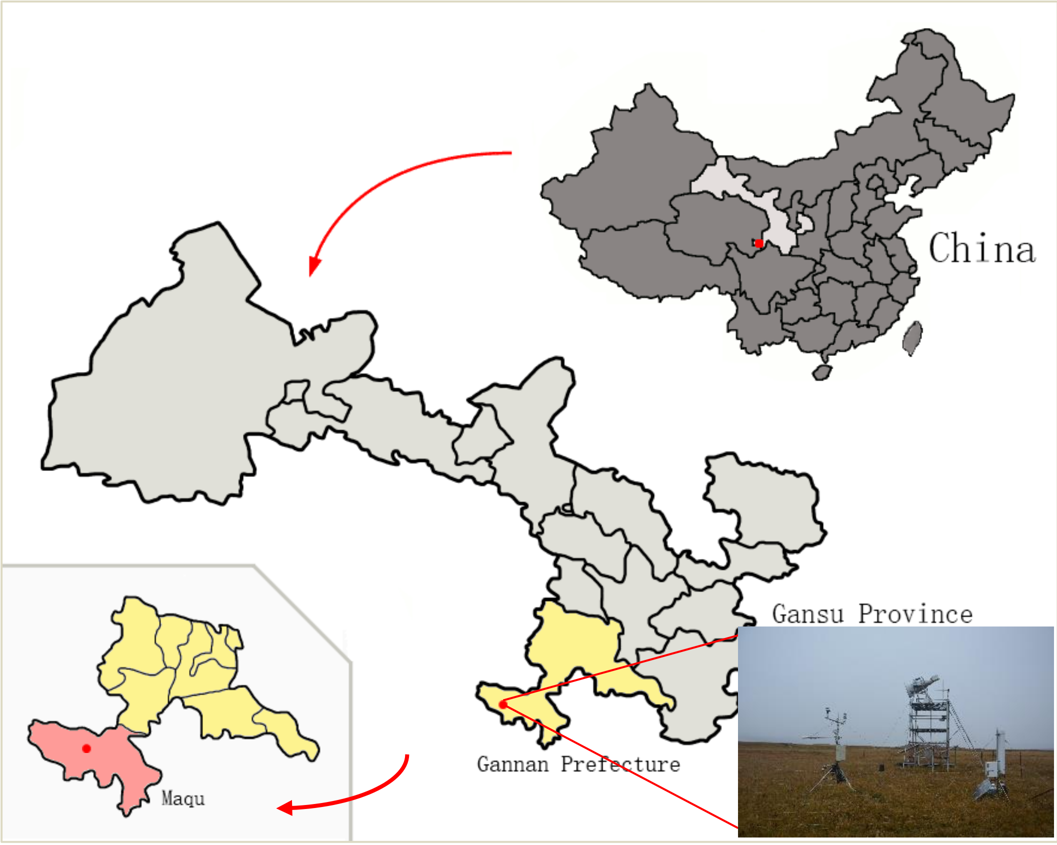

Figure 2-2 Location of Maqu County (pink area) and Gannan Prefecture (yellow area) within Gansu province, and the 3 red points indicate the location of CRP in the maps. The photo shows the scenery around the CRP (Source: http://sedac.ciesin.org/data/collection/cddc/sets/browse).

2.2. Data sets

The datasets for satisfying the study objectives come from three data sources, including the CRP, the Neutron Monitor Database (NMDB) and the point measurement (Table 2-2). And cosmic-ray neutron counts data and point measurement data of soil moisture and ST compose the most important datasets in this study. Additionally, the point measurement data is obligatory to acquire from the area within or near the footprint of the CRP.

Table 2-2 Required data and data source in this research

Data sources	Data	Units
CRP	Neutron counts measured by CRP	counts h^{-1}
	Air pressure	hPa
	Atmospheric water vapour	%
NMDB	Incoming cosmic-ray flux	counts s^{-1}
Point measurement	ST	°C
	USWC	m^3m^{-3}

2.2.1. Cosmic-ray neutron counts

The CRP records down the neutron counts along with some other variables like the atmospheric pressure, air humidity, air temperature and battery voltage in 15 minutes' interval (Appendix A shows a sample of original CRP output data). The atmospheric pressure, air humidity and air temperature participate in the correction of neutron counts for normalizing the correlation between soil water content and neutron counts. It should be noted that the measured neutron counts were not instantaneous measurements but were integrated measurements. Table 2-3 shows a sample of CRP output data items employed in this study.

Table 2-3 Typical data output from a CRP

Columns: 1	2	3	4	5
UTC	Moderated Neutron Counts	Air Pressure	Air Temperature	Relative Humidity
	N	P	T	U
yyyy-mm-dd h:m	cph	hPa	°C	%
2016/10/10 02:01:00	2094	673.03	2.9	100.0
2016/10/10 02:16:00	2073	673.23	3.0	100.0
2016/10/10 02:31:00	2040	673.35	3.2	100.0
2016/10/10 02:46:00	1995	673.52	3.2	100.0
2016/10/10 03:01:00	2031	673.47	3.7	100.0
2016/10/10 03:16:00	1980	673.59	3.7	99.7
2016/10/10 03:31:00	1977	673.60	3.9	99.4
2016/10/10 03:46:00	1920	673.82	4.0	99.9

where column numbers represent:

1. Date and time at end of record period in Universal Time
2. Counting rate from the moderated neutron channel in counts per hour
3. Barometric pressure
4. Air temperature
5. Relative humidity

2.2.2. Neutron Monitor Database

Since fast neutrons are generated by high-energy neutrons colliding with nuclei in the air and soil, the fluctuation of incoming high-energy neutrons intensity is necessary to depress the uncertainties of soil water content measuring. Figure 2-3 is a sample of the high-energy cosmic-ray neutron counts data after air pressure and efficiency correction from the NMDB (http://www.nmdb.eu/nest/search.php).

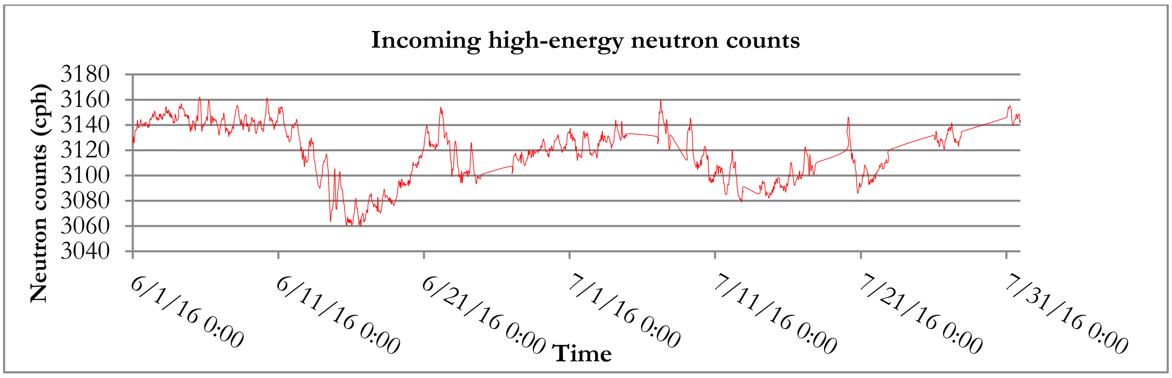

Figure 2-3 Hourly incoming high-energy neutron intensities measured with a neutron monitor at Tibetan Plateau in June and July 2016

2.2.3. Point measurement data

To improve and calibrate the COSMIC model, some soil properties should also be estimated by point measurement within or near the footprint of the probe as shown in Table 2-4. In this study, the soil water content is detected by the capacitance EC-TM ECH2O probe with a thermistor on it for detecting the temperature. Since the probe measuring the soil water content depending on measuring the dielectric permittivity of soil water and the dielectric permittivity of soil ice is much smaller than soil liquid water, thus the SIC is neglected when probe working (Evan, 1965; Jiang & Wu, 2004). SM/ST point measurement site is located at latitudes:33°53' N and longitudes 102°08' E, about 4 km to the CRP site. The depth of the probes is 5, 10, 20, 40 and 80 cm, respectively.

Table 2-4 A sample of point measured soil moisture at the study area with five depths ().

Time UTC+8	Port 1 m3/m3 VWC	Port 1 °C Temp	Port 2 m3/m3 VWC	Port 2 °C Temp	Port 3 m3/m3 VWC	Port 3 °C Temp	Port 4 m3/m3 VWC	Port 4 °C Temp	Port 5 m3/m3 VWC	Port 5 °C Temp
2016/1/1 0:00	0.079	-2.8	0.106	-2.2	0.122	-1.2	#N/A	#N/A	0.272	3.2
2016/1/1 0:15	0.078	-2.8	0.106	-2.1	0.123	-1.2	#N/A	#N/A	0.272	3.2
2016/1/1 0:30	0.078	-2.8	0.106	-2.2	0.123	-1.2	#N/A	#N/A	0.270	3.2
2016/1/1 0:45	0.078	-2.8	0.106	-2.2	0.123	-1.2	#N/A	#N/A	0.270	3.2
2016/1/1 1:00	0.078	-2.8	0.106	-2.2	0.123	-1.2	#N/A	#N/A	0.276	3.2
2016/1/1 1:15	0.078	-2.8	0.105	-2.2	0.122	-1.2	#N/A	#N/A	0.274	3.1
2016/1/1 1:30	0.078	-2.9	0.105	-2.3	0.123	-1.2	#N/A	#N/A	0.263	3.2
2016/1/1 1:45	0.078	-2.9	0.105	-2.3	0.122	-1.2	#N/A	#N/A	0.268	3.2

3. RESEARCH METHOD

3.1. Corrections of neutron counts

The raw neutron counts must be corrected for differences in air pressure, atmospheric water vapour, and the temporal variation of incoming cosmic-ray flux. Corrected neutron counts are attained from multiplying the raw counts by correction factors:

$$N_{COR} = N_{mea} \times F_i \times F_P \times F_w \quad \text{3-1}$$

where N_{COR} is the corrected moderated neutron count (Counts h^{-1}), N_{mea} is the raw moderated neutron count (Counts h^{-1}), F_i is the variation of incoming cosmic-ray flux correction factor, F_p is the air pressure correction factor, F_w is the atmospheric water vapour correction factor.

3.1.1. Incoming cosmic-ray flux correction factor

The secondary cosmic-ray intensity at the earth surface also depends on incoming primary cosmic-ray intensity (Desilets & Zreda, 2001). Therefore, pressure and efficiency corrected incoming primary cosmic-ray intensity provided by NMDB is used to eliminate this effect. The cosmic-ray neutron counts are usually normalized to a reference incoming cosmic-ray intensity as follows (M. Zreda et al., 2012):

$$F_i = I_{ref}/I \quad \text{3-2}$$

where *I* is incoming cosmic-ray intensity (Counts s-1). I_{ref} (Counts s-1) is a reference counting rate for the same neutron monitor from an arbitrary fixed point in time. The reference time for sensors in this study is 1 May 2011 (the same date used by the COSMOS network). Both this study and US-based COSMOS network access neutron flux data through the NMDB, which provides access to real-time data from a global network of monitoring stations.

A further complicating factor in neutron counts corrections is the fact that the strength of Earth's magnetic field at a given location also influences neutron flux intensity. At the poles the minimum energy that a particle must have to penetrate the Earth's magnetic field is less than that required near the equator. This minimum energy requirement is described as the cutoff rigidity (R_c) (Desilets & Zreda, 2003). For this reason, the neutron flux intensity correction for a location also needs to account for its geomagnetic cutoff rigidity. The way in which the CosmOz network and US-based COSMOS network achieve this differs and are compared in this paper. For the CosmOz network, the NMDB monitor with the closest cutoff rigidity to each CRP station was selected, following the reasoning that such sites will experience similar intensities of neutron flux. The COSMOS network follows a different approach by correcting all probes using one neutron monitor at Jungfraujoch, Switzerland and applying a correction for site cutoff rigidity (R_c)

$$R_{cCorr} = -0.075 * (R_c - R_{cJUNG}) + 1 \quad \text{3-3}$$

where R_{cJUNG} is the cutoff rigidity for the Jungfraujoch neutron monitor (4.49 Gv). This is a working model developed by the COSMOS project based on preliminary analysis of neutron monitor data from locations spanning a large range in R_c (Desilets & Zreda, 2001, 2003). The final cutoff rigidity-based intensity correction for COSMOS (f_{iRc}) has the form

$$f_{iRc} = (f_i\text{-}f) * R_{cCorr} + 1 \quad \text{3-4}$$

3.1.2. Air pressure correction factor

Correcting for differences in air pressure is essential since the incoming cosmic-ray neutron counts is attenuated with nuclei present in the atmosphere (Desilets & Zreda, 2003). F_p is calculated with the following equation:

$$F_p = e^{\left(\frac{P-P_0}{L}\right)} \quad 3\text{-}5$$

where e is the natural exponential and P is the measured air pressure (hPa) at the site during the moderated neutron count time. P_0 is a reference air pressure chosen to be the average air pressure during the field work execution (672.81 hPa, section 0). L represents the mass attenuation length (g cm^{-2}), which is a function of latitude and atmospheric depth (Desilets & Zreda, 2003).

3.1.3. Atmospheric water vapour correction factor

Since neutron counts are mainly related to the amount of hydrogen molecules in an area, raw moderated neutron counts must also be corrected for differences in atmospheric water vapour. Rosolem et al. (2013) found the following correction function for atmospheric water vapour:

$$F_w = 1 + 0.0054 \times \left(p_{vo} - p_{vo}^{ref}\right) \quad 3\text{-}6$$

where p_{v0} is the absolute humidity (g m^{-3}) at the site during the measurement time; p_{vo}^{ref} is the reference absolute humidity and was set to that of dry air (0 g m^{-3}).

3.2. N_0 method for obtaining soil water content from neutron counts

To simplify the relationship between neutron counts and average soil water content, Desilets et al. (2010) obtained a calibration curve for soil water content by fitting ground-level neutron fluxes simulated in MCNPX (Pelowitz, 2011) to the shape-defining function

$$(\theta_p + \theta_{lw} + \theta_{or}) * \rho_b = \frac{a_0}{\frac{N}{N_0} - a_1} - a_2 \quad 3\text{-}7$$

where θ_p is the gravimetric water content (kg kg^{-1}), θ_{lw} is the gravimetric lattice water content (kg kg^{-1}), θ_{or} is the gravimetric organic water content, ρ_b is soil bulk density (g cm^{-3}), N is corrected neutron counts (cph), N_0 is the counting rate over dry soil under the same reference conditions (cph), and a_0, a_1 and a_2 are fitting parameters. In the study by Desilets et al. (2010), a_0, a_1 and a_2 can be assigned the value of 0.0808, 0.372 and 0.115, respectively with a theoretic condition of homogeneous sand (SiO_2).

3.3. Cosmic-ray Soil Moisture Interaction Code

According to the physic process of fast neutrons generation and emission in the soil, three assumptions were proposed to simplify the relationship between neutron counts and depth-weighted soil moisture content (a) degradation of the incoming high-energy neutron flux with soil depth, (b) creation of fast neutrons at each depth in the soil, and (c) scattering of the resulting fast neutrons before they reach the soil surface, all of which processes may have parameterized dependency on the chemistry and moisture content of the soil. The newly-developed COSMIC was adopted as the forward observation operator to simulate the equivalent neutron count rates from simulated soil moisture profiles (i.e., soil moisture contents for 1000 vertical model layers of CLM from surface to 0.3 m depth) (X. Han et al., 2015; Shuttleworth, Rosolem, Zreda, & Franz, 2013) and takes into account the weighted contribution of individual soil layers with depth. The COSMIC operator calculates the number of fast neutrons reaching the CRP N_{COSMIC} at a near-surface measurement point by the equations below:

$$N_{COSMIC} = N\int_0^\infty \left\{A(z)[\alpha\rho_s(z) + \rho_w(z)]exp\left(-\left[\frac{m_s(z)}{L_1} + \frac{m_w(z)}{L_2}\right]\right)\right\} \mathrm{d}z \quad 3\text{-}8$$

$$A(z) = \left(\frac{2}{\pi}\right)\int_0^{\pi/2} exp\left(\frac{-1}{\cos(\gamma)}\left[\frac{m_s(z)}{L_3} + \frac{m_w(z)}{L_4}\right]\right) \mathrm{d}\gamma \quad 3\text{-}9$$

$$\alpha = 0.405 - 0.102\times\rho_s \quad 3\text{-}10$$

$$L_3 = -31.76 + 99.38\times\rho_s \quad 3\text{-}11$$

where N (counts/h) is the number of high-energy neutrons at the soil surface, z is the soil layer depth (m), α is the ratio of fast-neutron creation factor, ρ_s is the dry soil bulk density (g cm^{-3}), ρ_w is the total soil water density, including the lattice water (g cm^{-3}); $m_s(z)$ and $m_w(z)$ are the integrated mass per unit area of dry soil and water (g cm^{-2}), γ is the angle between the vertical below the detector and the line between the detector and each point in the plane (Shuttleworth et al., 2013), L_1 is the high energy soil attenuation length with value of 162.0 g cm^{-2}, L_2 is the high energy water attenuation length of 129.1 g cm^{-2}, L_3 is the fast neutron soil attenuation length (g cm^{-2}) and L_4 is the fast neutron water attenuation length with value of 3.16 g cm^{-2} (Shuttleworth et al., 2013).

3.4. Footprint and meassuring depth of CRP

3.4.1. Footprint

The footprint of CRP covers the area in which the soil water content influence the probe recorded results. Since the origination of neutron counts detected by the CRP is not definitely defined, its footprint is normally designed as the area in which 86% (1-e^{-2}) of the detected neutrons originate (Trenton E. Franz, Zreda, Rosolem, & Ferre, 2012; Marek Zreda et al., 2008). To simplify the procedure for deucing the footprint, some researchers assumed that fast neutron particles diffusive homogenously (M. Zreda et al., 2012; Franz et al., 2012). Under this assumption, the footprint of CRP is decided by the air pressure, weakly related to SWC and the othet factors (Desilets & Zreda, 2013). And the radius of CRP footprint could be calculated by equation 3-12

$$\mathrm{R} = R_0 * \left(\frac{P_0}{P}\right) \quad 3\text{-}12$$

where R (m) is the footprint radius at air pressure P (hPa), and R_0 is the reference radius (300 m) at the reference air pressure P_0 (a standard air pressure at sea level, 1013 hPa) (Zreda et al., 2008).

However, a new study by Köhli et al. (2015) found that the diffusion of fast neutron particles is not homogenous, since the air humidity, SWC and vegetation can moderates the fast neutron propagation. As a result, the air humidity, SWC and vegetation are also three significant factors for deciding the footprint. And the footprint radius considering these two factors is estimated as equations below:

$$f_{veg}(\theta) = 1 - 1.07(1 - e^{-0.41H_{veg}})(1 + e^{-7\theta}) \quad 3\text{-}13$$

$$f_p = \frac{0.5}{0.86 - e^{-P/P_0}} \approx P/P_0 \quad 3\text{-}14$$

$$R(h,\theta,p,veg) = f_p * f_{veg}(\theta) * R(h,\theta) \quad 3\text{-}15$$

where, H_{veg} (m) is the crops of height; θ is the SWC (m^3 m^{-3}), $R(h,\theta,p,veg)$ is the footprint radius considering the influences of air humidity, SWC, air pressure and vegetation. f_p is the air pressure scaling factor, $f_{veg}(\theta)$ is the vegetation scale factor, $R(h,\theta)$ is the footprint radius influence only by the air humidity and SWC, with a standard air pressure at sea level (1013 hPa) and no vegetation. As the results of $R(h,\theta)$ is hard to explain with mathematic methods, its results are presented as contour in Figure 3-1.

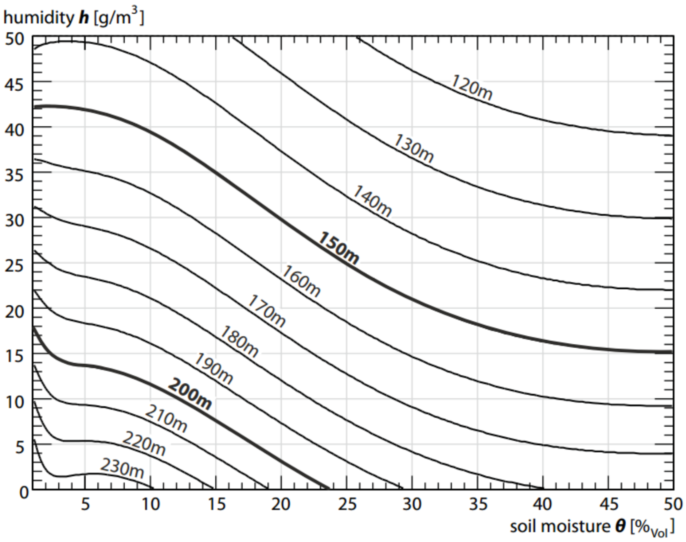

Figure 3-1 Footprint radius $R(h,\theta)$ and its dependency on soil moisture and air humidity at sea level (Köhli et al., 2015).

3.4.2. Depth

The same to the footprint, the depth of CRP is also not naturally defined but designed as the near ground surface part of soil in which 86% of the detected neutrons originate. The fraction of fast neutron counts for each depth follows an exponential decay over the soil depth. And a simplified method for calculation the CRP depth is induced as equation 3-16.

$$Z = \frac{5.8}{\theta_g + \theta_{lw} + \theta_{or} + 0.0829} \quad \text{3-16}$$

where ρ_{bd} is the soil bulk density (g cm^{-3}), θ_{lw} is the volumetric lattice water content (kg kg^{-1}), θ_{or} is the volumetric organic water content and θ_g is the soil volumetric water content (kg kg^{-1}).

The COSMIC model is a simplification of Monte Carlo N-Particle eXtended (MCNPX) model, depending on the neutron propagate characteristics. This model can calculate the fraction of neutron counts of specific depth to the total neutron created in the soil. According to this property, the COSMIC could indicates the depth of its simulating area in a relatively high accuracy.

3.5. Time window for data smoothing

According to the generation of fast neutrons, these particles propagate randomly to different directions, leading to a temporal fluctuation. Mainly caused by the short interval of 15 minutes, this fluctuation of neutron counts does not correspond to the temporal variations of soil moisture. To make the soil water content from neutron counts reflects the reality, the data require a preprocess to depress the influence of this particles propagation randomly. However, it is not feasible to smooth the soil water content directly for removing the deviation from neutrons' randomness, since the soil water content itself is changing with time. Here, a compromise method is to compare the smoothed soil water content from neutron counts with soil water content from point measurement, disregarding the original disparity between these two kinds of soil water content with both 15 minutes' interval. In this study, moving average method is employed to diminish the fluctuation of soil water content caused by the randomness of neutron propagation. And the sensitive analysis for the time window of moving average method is made with 10 different values (30 minutes, 1 hour, 2 hours, 3 hours, 4 hours, 6 hours, 8 hours, 9 hours, 12 hours and 24 hours). And these 10 different time windows are selected based on respecting the fact of diurnal fluctuation of soil water content (Jackson, 1973)

To achieve the sensitive analysis of moving average time window, three objective functions, the correlation coefficient (R^2), the Nash-Sutcliffe coefficient of efficiency (NS) (Nash & Sutcliffe, 1970) and the Relative Volume Error (RVE) are used, illustrating the performance of two kinds of soil water content from 3 aspects (as Table 3-1). The soil water content from point measurement is treated as the observed data, while the soil water content from neutron counts is treated as a simulation to point measurement data.

Table 3-1 The characters of the three objective functions for time window setting

	Range	Optimal value	Main function
R^2	[0,1]	1	Correlation
NS	(-∞,1]	1	Tendency balance
RVE	(-∞,+∞)	0	Mass balance

R2 is a popular function indicates the correlation between two sets of values. It returns the square of Pearson product moment correlation coefficient (Excel, n.d.), ranging from 0 to 1. A higher the value of this function means a better correlation between two data sets, while value 1 and 0 indicate the best and worst fit, respectively.

As one of the important measures for predictive power of hydrological model performance, in this study, NS function is adopted to evaluate the tendency synchronism of the two water content. The NS value can range from $-\infty$ to 1. NS equal to 1 indicate a perfect simulation; NS ranging between 0.9 and 1 indicates model performs extremely well; NS ranging between 0.8 and 0.9 indicates model performs very well; NS ranging between 0.6 and 0.8 indicates model performs reasonably well; Negative NS indicates the observed mean discharge is a better predictor than the model simulation. On the hydrography the shape of simulation result is measure by NS.

RVE is also a commonly applied measurement about the mass balance error between the observed and the simulated counterparts. The RVE value can range from $-\infty$ to $+\infty$. The value equal to 0 indicates a best performance of the mass simulation and the closer to 0, the better the mass simulation would be. A relative volume error between +5% and -5% indicates that a model performs well. RVE ranging between +5% and +10% or -5% and -10% indicates a reasonable performance of simulation. However, even though a very good volume could not assert the simulation is well fit to observation, since the RVE can only evaluate the simulation of the total volume.

The 3 objective functions are explained as equation 3-17, 3-18 and 3-19 in this study.

$$R^2 = \sum_{i=1}^{n}\left(\left(Q_{n,i} - \overline{Q_c}\right)^2 * \left(Q_{p,i} - \overline{Q_p}\right)^2\right) / \left(\sum_{i=1}^{n}\left(Q_{n,i} - \overline{Q_c}\right)^2 * \sum_{i=1}^{n}\left(Q_{p,i} - \overline{Q_p}\right)^2\right) \quad 3\text{-}17$$

$$NS = 1 - \sum_{i=1}^{n}\left(Q_{n,i} - Q_{p,i}\right)^2 / \sum_{i=1}^{n}\left(Q_{p,i} - \overline{Q_p}\right)^2 \quad 3\text{-}18$$

$$RVE = \left(\sum_{i=1}^{n}\left(Q_{n,i} - Q_{p,i}\right) / \sum_{i=1}^{n} Q_{p,i}\right) \times 100\% \quad 3\text{-}19$$

where i is the observing sequence, n is total the number of observations, $Q_{n,i}$ is the soil water content derived from observed neutron counts, $Q_{p,i}$ is the soil water content from point measurement. $\overline{Q_n}$ and $\overline{Q_p}$ represent the average of soil water content from neutron counts and point measurements, respectively.

3.6. The correlation between ST and LSWC in frozen soil

Although the independence between LSWC and TSWC is not yet proved in the frozen soil and debates still exist for this problem (Kurylyk & Watanabe, 2013). However, plenty of experiment result and in-situ data implies a high correlation between the LSWC and ST under frozen ground (Musa et al., 2016; Civan, 2000; Bronfenbrener & Bronfenbrener, 2012;). In fact, this high correlation is a supplementary specification for the independence between the LSWC and TSWC under frozen ground, since ST and TSWC are weekly connected with each other. In this study, we ignore the relationship between TSWC and LSWC and focus on the correlation model between ST and LSWC.

The correlation between ST and LSWC in frozen soil is simulated by various models by former researchers. Within this models, two popular fit functions are the power function and the exponent function with many variants based on them (Kozlowski, 2007; Brooks & Corey, 1966; Hansson, Šimůnek, Mizoguchi, Lundin, & Van Genuchten, 2004; McKenzie, Voss, & Siegel, 2007).

Anderson and Tice (1973) adopted the power law empirical correlations to briefly describe this relationship as equation:

$$\theta_l = \alpha(-\varepsilon^{\beta}) \qquad 3\text{-}20$$

where, θ_l (m^3 m^{-3}) is the LWSC; α and β are fitting parameters being dependent on basic soil types; ε represents how much ST lower than the freezing temperature of pure water given by:

$$\varepsilon = T_t - T \qquad 3\text{-}21$$

where T (°C) is ST T_t is the freezing temperature of pure water (0 °C at 1 atm).
Using average thermal properties of the soil constituents, Civan (2000) and derived an approximate analytical exponential solution, which is sufficient for all practical purpose:

$$\theta_l = \theta_a + (\theta_t - \theta_a) * exp(-k\varepsilon) \qquad 3\text{-}22$$

where θ_l is mass of the unfrozen water per unit mass of dry soil (g g^{-1}); θ_o and θ_a denote the total water masses per unit mass of dry soil (g g^{-1}) (the total water masses is fixed in this experiment) and the adsorbed water masses per unit mass of dry soil (g g^{-1}) and k is the freezing rate coefficient.

In this study, these two functions and some of their variants would be employed to fit the point measurement data to find an optimal function for the ST and LSWC. After the function fixed, it would be invoked to retrieval the LWSC from ST and simulate the FT process at Tibetan Plateau.

3.7. SIC derivation

The relationship between TSWC, LSWC and SIC is expressed as equation 3-23, neglecting the exist of water vapour in the soil. In addition, the distortion caused by water freezing is also neglected, and the SIC is simply expressed as ice water equivalent.

$$\theta_t = \theta_l + \theta_i \qquad 3\text{-}23$$

where θ_t indicates the TSWC (m^3 m^{-3}), θ_l indicates the LSWC (m^3 m^{-3}), θ_i indicates the SIC (m^3 m^{-3}). It should be noted that the density differences between ice and water are ignored and the ice is turn into liquid water equivalent here for calculation convenience.

With this equation, the SIC is available, since the CRP neutron counts can retrieval the TSWC with an integral value, and the SM/ST point measurement can record the LSWC when the soil is frozen.

3.8. Flowchart

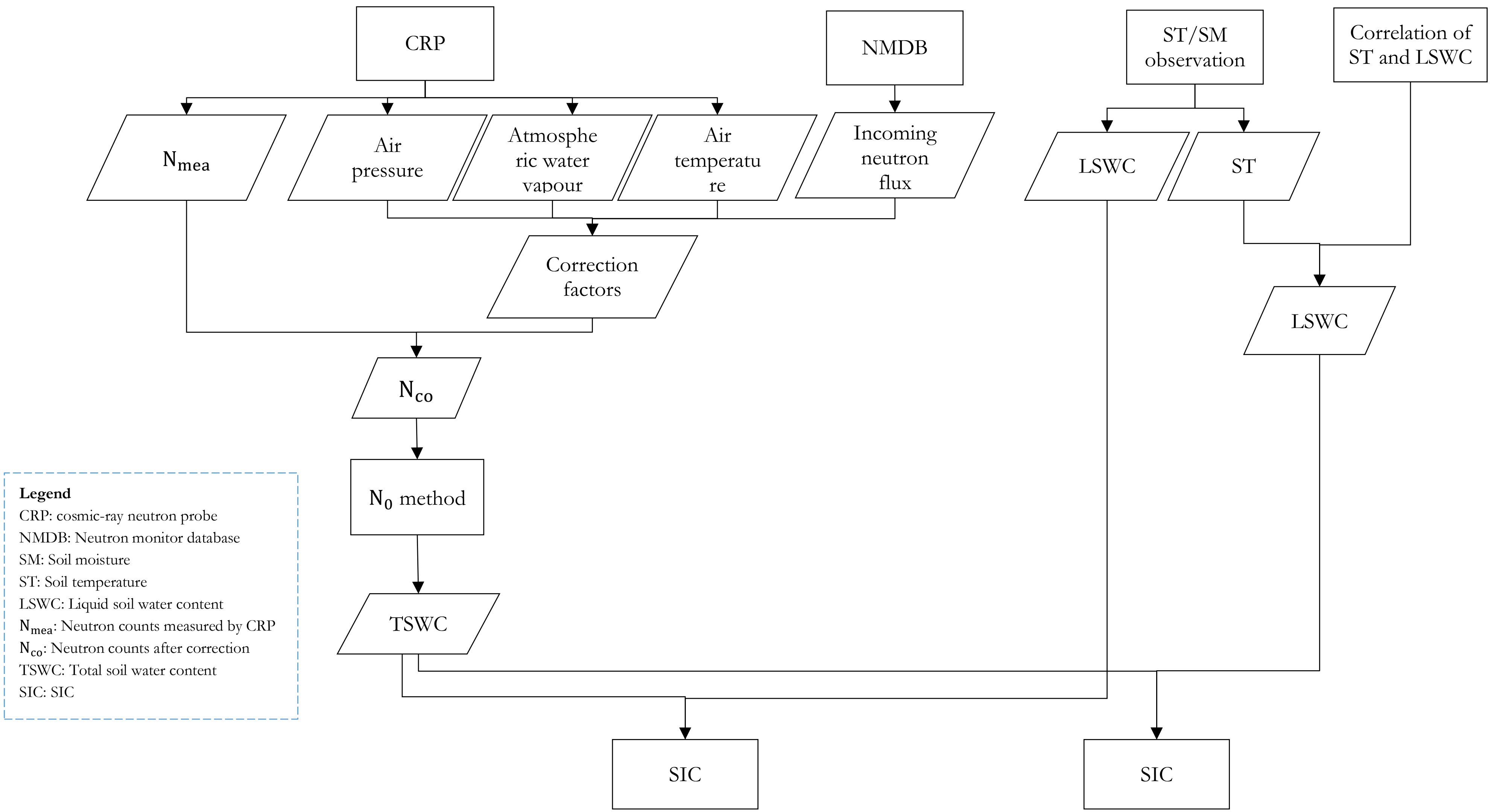

Figure 3-2 Flowchart of research methodology

4. FIELD WORK

Before the cosmic-ray rays reach the CRP, temporal changes of the in air pressure, atmospheric water vapor and incoming neutron flux will all influence the result of neutron counts recorded by the CRP. Furthermore, since other atoms existed in the soil excepting hydrogen can also attenuate fast neutron, the influence of dry soil need us to pay attention to. The second kind of atoms which can attenuate the fast neuron effectively is carbon atom, with one-sixth the attenuation ability of hydrogen. And in some area, the carbon atoms can be abundant in the soil. As a result, pressure, atmospheric water vapor and incoming neutron flux are required to record with neutron counts and the dry soil density is required to record down accompany with neutron counts in calibration, as well as in the normal measurement.

Like all methods, the cosmic-ray method has potential limitations. One possible problem is the presence in the footprint of hydrogen other than that in soil water, for example in hydrous minerals (clay minerals, hornblende, gypsum, etc) or in vegetation and soil organic matter (M. Zreda et al., 2012). Although, these limitations are small enough to be implicitly embedded in local calibration, it would be better to find out how much of these limitations influence the result in the calibration.

4.1. Field work plan

4.1.1. Site Locations

The CRP was installed at the point with coordinate: 33°54'59.55"N, 102° 9'32.50"E. To measure the soil water content in the footprint of the CRP, Soil water content of 18 point locations are chosen. The soil sample is collected at 5 depths (0-5, 5-10, 15-20, 25-30 and 35 -40 cm) for 9 locations. The sample locations are every 60 degrees (30, 90, 150, 210, 270 and 330) for radii of 25 m and every 120 degrees (60, 180 and 300) for radii of 75 m. The ECH_2O probe observation is also processed at 5 depths (0-5, 5-10, 15-20, 25-30 and 35 -40 cm) for 9 locations. And the ECH_2O probe observation location are every 120 degrees (0, 120 and 240) for radii of 75 m and every 60 degrees (30, 90, 150, 210, 270 and 330) for radii of 200 m (Figure 4-1and Table 4-1).

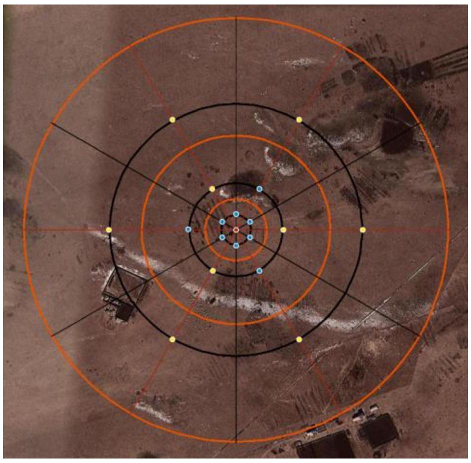

Figure 4-1 Distribution CRP site (red point), 9 soil sampling sites (blue points) and 9 ECH2O probe observing sites (yellow points) in the field work plan (The locations on google map: https://drive.google.com/open?id=1kpRxftY-890W_OU6jJvbFZ3nAEM&usp=sharing).

Table 4-1 Location of the soil sample point and sensor measure point

Site	Latitude	Longitude	Degree	Radii (m)
CRP	33°54'59.55"N	102°9'32.50"E	–	0
SP1	33°55'0.336"N	102°9'32.47"E	0	25
SP2	33°54'59.94"N	102°9'33.31"E	60	25
SP3	33°54'59.11"N	102°9'33.31"E	120	25
SP4	33°54'58.72"N	102°9'32.47"E	180	25
SP5	33°54'59.11"N	102°9'31.61"E	240	25
SP6	33°54'59.94"N	102°9'31.61"E	300	25
SP7	33°55'1.596"N	102°9'33.91"E	30	75
SP8	33°54'57.42"N	102°9'33.91"E	150	75
SP9	33°54'59.54"N	102°9'29.52"E	270	75
EC1	33°54'57.42"N	102°9'35.35"E	90	75
EC2	33°54'59.54"N	102°9'31.00"E	210	75
EC3	33°55'1.596"N	102°9'31.00"E	330	75
EC4	33°55'5.124"N	102°9'36.32"E	30	200
EC5	33°54'59.54"N	102°9'40.21"E	90	200
EC6	33°54'53.93"N	102°9'36.32"E	150	200
EC7	33°54'53.93"N	102°9'28.58"E	210	200
EC8	33°54'59.54"N	102°9'24.66"E	270	200
EC9	33°55'5.124"N	102°9'28.58"E	330	200

4.1.2. Tool list

- Soil Sampler equipment, including: Sample rings, extension and handle crossbar
- GPS for confirming the site point location
- Knife for incising the redundant soil out of the soil sample ring and cut the grass
- Rubber or plastic mallet for striking the top of the soil sampler
- Balance (accurate to 0.01g)
- Marker pen for making the label on the soil sample ring
- Electrical tape for sealing the caps
- Black boxes for keeping the soil samples more safely
- Shovel for digging the soil if needed
- Soil weight and soil bulk density worksheet
- Drying oven
- ECH_2O probe
- Pen for recording the experiment results
- Blank paper for writing down some unexpected information
- Rain coat and rain boot

4.1.3. Calibration contents

Soil samples are collected within the probe footprint with soil sample ring. Soil moisture is measured using the oven-drying method, and area-average soil moisture is computed. Only 9 sample points, other than typical 18 sample points are selected to reduce the destruction to the environment around the station. To guarantee the quality of the calibration, ECH_2O probe are adopted to detect the soil moisture at the left 9 sample points. shows the distribution of CRP, 9 soil sample pointes and ECH_2O probe points.

The key information required to calibrate the probe, in ascending order of importance, are:

(1) Soil water content (typically volumetric water content)

(2) Soil bulk density

(3) Clay structural (lattice) water
(4) Soil organic carbon
(5) Standing wet and dry biomass

Note that in soils with a sandy texture, (3) and (4) can be neglected, (2) can usually be determined with a small number of samples, and (5) vegetation changes are often small over the season in which case they can be ignored.

4.1.3.1. Volumetric water content and soil bulk density

The spatial distribution of pore (gravimetric) water can be highly variable, requiring many samples in order to get an accurate spatial average. The gravimetric campaign consisted of averaging individual samples as . This pattern was chosen such that each sample location (and representative area) is given equal weight in the CRNP sensitivity (sensitivity dies off exponentially from sensor). Note that the sample locations don't need to be located within a several meters of the targeted location are sufficient, so long as sample locations are not biased by human judgment.

As a practical matter, retaining undisturbed samples can be difficult with any coring apparatus. However, it is recommended that at least one undisturbed sample is taken so that the volume of each soil core section is accurately known. Then the soil bulk density and volumetric water content can be estimated by gravimetric methods. The standard gravimetric method is to obtain the wet soil weight and dry soil weight following oven drying at 105 ℃ for about 48 hours until weight is constant(ASTM D2216-10, 2010; T. E. Franz, Zreda, Rosolem, & Ferre, 2013).

Note: while in the field, always tape around the seam of the filled soil can to prevent unwanted drying or soil losses of the samples.

4.1.3.2. Structure water and soil organic carbon

These are determined on a subset of the samples collected for water content and bulk density. Structural water is water contained in the mineral lattice of clay particles, and hence is higher in clay-rich soils (data base is available relating soil texture to lattice water which enable the calculation of lattice water from measured soil texture). Soil organic carbon water equivalence is the amount of water contained in the organic carbon compounds assuming the compounds are cellulose ($C_6H_{10}O_5$). These analyses can be done by commercial laboratories. For expedience, it is acceptable to create one composite sample for analysis by the commercial laboratory. Following oven drying and weighing of the gravimetric water samples, this composite sample can be created by taking approximately 1 g from each sample can.

4.1.3.3. Vegetation in study area

One can either set out a 50x50 cm sampling square or calculate the number of plants per unit area. A common practice is to sample 5-7 locations around the CRNP footprint. For biomass sampling, it is best to cut the vegetation near the ground surface and then place it in a brown paper bag. Then weigh the wet sample, and place the sample in an oven at 75 ℃ for about5 days until the weight is stable to determine the dry weight of the sample(O'Kelly, 2004). With this information, calculation of the mass of water and the mass of dry plant can be determined. The water equivalent of dry plant (cellulose) to water is the dry weight multiplied by 0.5556 (A. Wahbi, 2015).

4.1.4. Operation steps

4.1.4.1. Procedure for collecting soil samples

To finished the field calibration work fluently, the operation procedures are list chronologically below:

Confirm the location of each site point in the filed using GPS and its coordinate;
Cut the grass near the ground surface for convenience of sample collecting and collect them for calculating the mass of biomass;
Use the soil sample ring to collect soil in each five depths;
Package the soil in soil sample ring by setting up two caps on both ends;
label the ring;
Repeat this steps until 9 points all finished

4.1.4.2. Procedure for drying soil

Remove the plastic lids from the rings containing the samples and wrap the bottom of the rings with small pieces of aluminium foil. If soil samples are contained in jars, then remove the lid.
Set the samples in a 105°C oven and allow them to dry until a constant weight is reached. Typically, leaving the samples in the oven overnight is sufficient however; leaving them in the oven longer will not present any problems.

Remove the soil from the Soil Sampler rings and foil, or glass jars, and weigh dry soil samples. Record the weights in the "Dry Soil Weight" column of the Soil Bulk Density Worksheet. (NOTE: Sample bulk densities are automatically calculated once the sample soil dry weights are entered into the workbook.)
Put un-weighed samples back in the oven until sample preparation can be resumed.

4.1.4.3. Procedure for observing soil water content with ECH2O probe

Confirm the location of each site point in the filed using GPS and its coordinate;
Cut the grass near the ground surface for convenience of sample collecting and collect them for calculating the mass of biomass;

Set the sensor at 5 different depths (2.5, 7.5, 17.5,27.5 and 37.5 cm, represent for the ranges: 0-5, 5-10, 15-20, 25-30 and 35-40 cm) to measure the soil water content; Repeat this steps until 9 points all finished.

4.1.5. Conclusion of field work plan

In this plan the main contents are about procedures for field calibrating a CRP using independent soil measurements. This involves using soil sample rings to take 45 of volumetric soil samples at 9 sample points around the sensor, with every sample take 5 cm of soil in depth. Also ECH_2O probe is adopted to detect the soil water content in 9 sensor points. Since clay lattice water content and soil organic carbon content derivation is realized in more complicated experiments, these two items are neglected in the calibration. Standing wet and dry biomass is also plan to measure in order to improve the accuracy of the soil moisture determination. A schedule for arranging the work in the field is presented in Appendix A.

4.2. Field work result

4.2.1. Soil sampling result

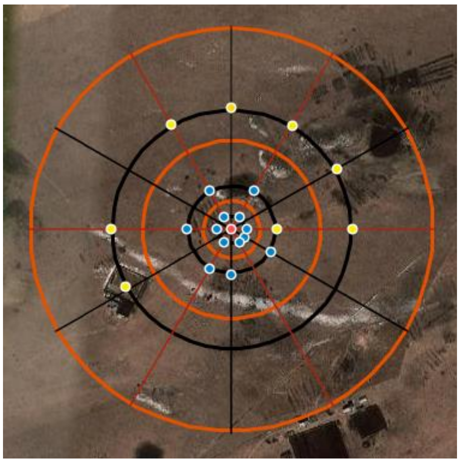

Figure 4-2 Distribution CRP sites (red point), 13 soil sampling and theta probe observing sites (blue points) and 8 theta probe observing sites (yellow points) in the field work execution (The locations on google map: https://drive.google.com/open?id=1CBb5eJuhkZ48YpH2Lr3UEqNkr2Y&usp=sharing).

The field work was executed in 10th October 2016, within the probe foot print of the CRP locates in Maqu. There are some differences between the field work execution and field work plan. Firstly, the ECH_2O was replaced by the theta probe, which is much more convenient than the ECH_2O to observe the soil water content; secondly, the theta probe only observed the soil water content at the ground surface, rather than 5 various depths to represent for 5 ranges as planned for ECH_2O probe; thirdly, the observation sites for soil sampling was increased to 13 and theta probe was applied to 21 sites (13 sites accompanied by soil sampling and 8 sites executed alone) as Figure 4-2; fourthly, the observation sites are not according to the plan exactly, since environment is complicated in the field.

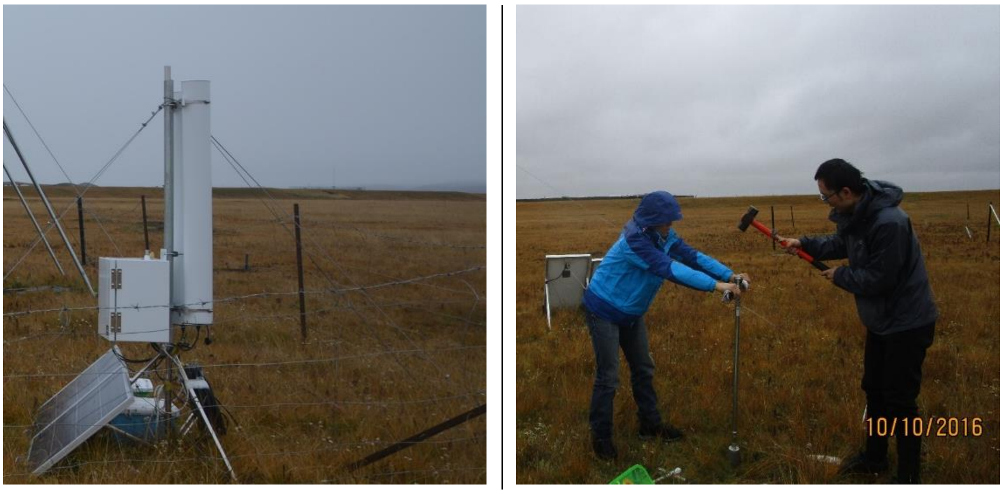

Figure 4-3 The CRP located in Maqu (left) and Soil sampling in the field (right)

Table 4-2 Information of CRP site

	Value	Unit
Site name	Maqu	-
Latitude	33°54'59.55"	°N
Longitude	102° 9'32.50"	°E
Elevation (m)	3436	m
UTC Time Zone	8	hours
Calibration Date	2016-10-10	UTC+8
Calibration Time	10:00-19:16	UTC+8

In this study the soil ring used is in the criterion of 100 cm^3, with the ring weights were obtained beforehand. In order to get the soil water content, the weight of wet soil with ring was obtained after sampling and the weight of dry soil with ring was obtained after oven drying. In addition, the water content in standing biomass was also taken into account to remove its effect to the soil water content.

$$\rho_b = (W_{d+r} - W_r) / V_r \qquad 4\text{-}1$$

$$\theta_p = W_{w+r} - W_{d+r} \qquad 4\text{-}2$$

$$\theta_g = \theta_p / \rho_b \qquad 4\text{-}3$$

$$\rho_{sb} = (W_{wsb} - w_{dsb}) / (S_{sb} * H_{sb}) \qquad 4\text{-}4$$

Where, ρ_b is the soil bulk density; W_{w+r} and W_{d+r} represent the weight of wet soil samples after sampling with soil ring and dry soil samples after oven drying (105 °C) with soil ring, respectively; W_r and V_r represent the weight and volume of soil ring, respectively; θ_p and θ_g represent the volume soil water content and the gravimetric soil water content ; ρ_b is the soil bulk density; ρ_{sb} is the water content of standing biomass; W_{wsb} and W_{dsb} represents the weight of wet standing biomass right after sampling and the weight of dry standing biomass after oven drying (75 °C), respectively; S_{sb} and H_{sb} represents area and average height of standing biomass sampling (the average height of standing biomass is assumed 15 cm here), respectively.

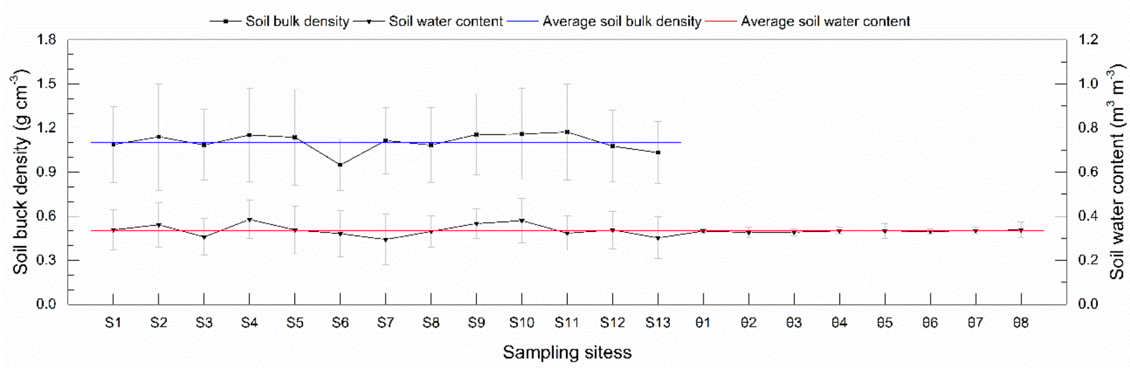

Figure 4-4 The soil sampling results of soil bulk density (square points) and SWC (triangle points) with one standard deviation compared to the average soil bulk density (red line) and SWC (blue line) during soil sampling period from10:00 to 19:16 on 10th October 2016

Table 4-3 Soil sampling results

	Maximum	Minimum	Mean	Standard deviation	Coefficient of variation (%)
Soil bulk density	1.1728	0.9496	1.1039	0.0595	5.39
Soil water content	38.5840	29.4580	33.5657	2.2211	6.62

By invoking equations 4-1, 4-2, 4-3 and 4-4, the soil water content, soil bulk density and water content of standing biomass could be derived. It is noteworthy that above ground biomass was figured out to be only 0.715 kg/m^2 , when the grass was still moisture (October), so it is neglected in CRP result calculation in this study. Considering the time limitation, the soil lattice water and soil organic water were not measured in the field work. A value of 0.03 (m^3 m^{-3}) was assumed for the lattice water content in the study area (Trenton E. Franz, Zreda, Rosolem, et al., 2012; X. Han et al., 2015). And a value of 0.01 (m^3 m^{-3}) was assumed for the organic soil water content according to the study by Su et al. (2011).

4.2.2. CRP measuring result

While the soil sampling work was executing, the CRP was also working, recording down the neutron counts and other related variables. Among the CRP recorded data, the average air pressure during the soil sampling is employed to correct the neutron counts (section 3.1.2) and the corrected average neutron counts is necessary for the calibration of CRP (Figure 4-5).

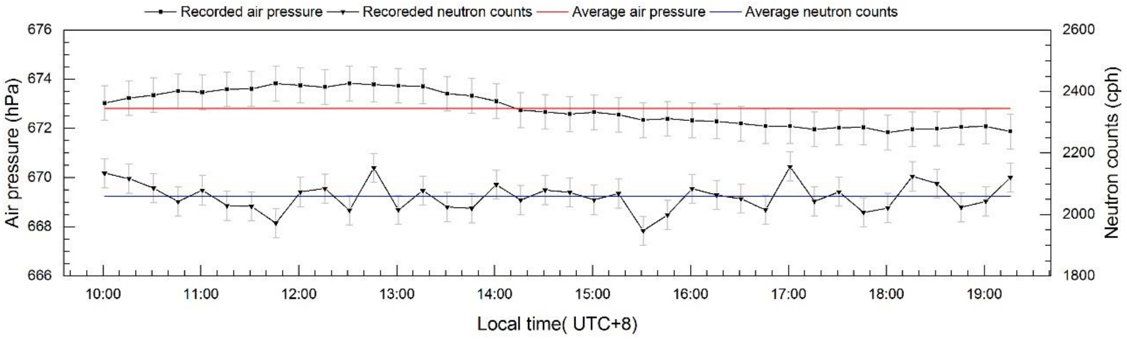

Figure 4-5 The CRP recorded neutron counts (triangle points) and air pressure (square points) with one standard deviation compared to the average neutron counts (blue line) and air pressure (red line) during soil sampling period from10:00 to 19:16 on 10th October 2016.

Table 4-4 Result of CRP data recorded during soil sampling

	Maximum	Minimum	Mean	Standard deviation	Coefficient of variation (%)
Average air pressure	673.8300	671.8400	672.8074	0.6962	0.10
Corrected neutron counts	2156.1478	1947.1268	2058.6345	46.7531	2.27

5. RESULT AND ANALYSIS

5.1. CRP calibration

5.1.1. N_0 method calibration

N_0 is an instrument specific calibrated parameter that represents the count rate over dry soils (cph). Depending on N_0, neutron counts can be convert to soil water content with equation 3-7. Thus, to calibrate the CRP with N_0 method is to evaluate N_0 value.

After the field work was executing, the CRP was also running, with the corresponding neutron counts and related correction factors recorded at the same time. After the correction of neutron count (details will be explained in section 3), the average of corrected neutron counts during the field work execution is 2058.63 (cph) (Figure 4-5). Invoking the known θ_p, N value during field work and the assigned a_0, a_1, a_2 value into equation 3-7, results in N_0: 3913.1263 (cph).

5.1.2. COSMIC method calibration

After the soil sampling, the soil bulk density ρ_b is known, so it is available to get the value of α and L_3 via 3-10 and 3-11. So far, the parameters for COSMIC model are all obtained except N(Table 5-1).

Table 5-1 parameters for COSMIC model

Parameter	Symbol	Value	Unit
Ratio of Fast Neutron Creation Factor (Soil to Water)	*N*	671.2447	cph
High Energy Soil Attenuation Length	*L1*	162	g cm^{-2}
High Energy Water Attenuation Length	*L2*	129.1	g cm^{-2}
Fast Neutron Soil Attenuation Length	*L3*	74.92	g cm^{-2}
Fast Neutron Water Attenuation Length	*L4*	3.16	g cm^{-2}

The high-energy neutron counts parameter *N* of the forward COSMIC model needs to be calibrated first by using soil water content derived from the soil sampling and the average neutron counts measured by the CRP during the soil sampling. The optimal parameter *N* should result in the best-fitted neutron count simulation from COSMIC compared with the measured neutron counts, and then, it was used for soil moisture assimilation. For the CRP in our study area, the optimal value of *N* was obtained as 671.2447 (cph). Furthermore, with the optimized high-energy neutron counts parameter N, the COSMIC model can get the value of corresponded neutron counts over dry soils and the result is 3934.2372 (cph). The deviation of the N_0 from COSMIC model to N_0 from N_0 method is: 0.5395%. This small deviation may assistant to persuade the accuracy of both N_0 method calibration and COSMIC model calibration.

5.2. TSWC from neutron counts

Before the calculation of TSWC, the neutron counts is corrected for the incoming flux, air pressure, atmospheric water vapor and in coming flux as mentioned in section 3.1 (Figure 5-1).

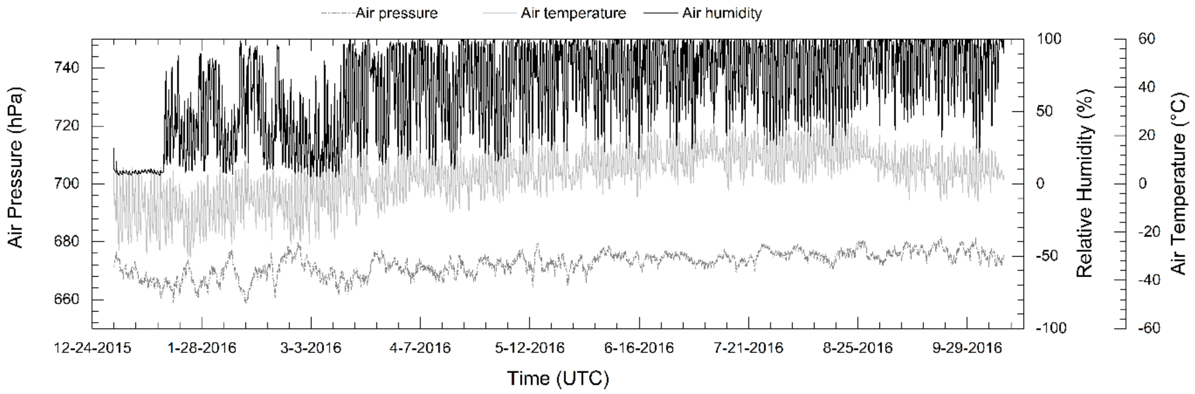

Figure 5-1 The air pressure, air temperature and air humidity recorded by CRP for neutron correction.

The soil water content is inversely correlated to the corresponding CRP neutron counts, so form the recorded CRP results, it is possible to calculate the soil water content. The equation 3-7 is a universally applied method to figure out the soil water content from cosmic-ray neutron counts. As the soil bulk density and N_0 are respectively obtained in section 4.2.1 and 5.1.1, the soil water content can be retrieval from the neutron counts directly (Figure 5-2).

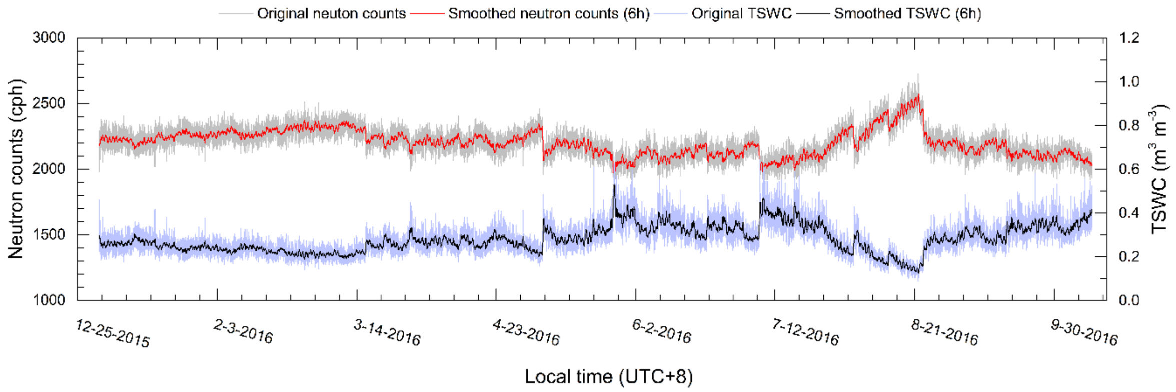

Figure 5-2 The neutron counts and soil water content. Black line indicates the original neutron counts from CRP; the blue line indicates the smoothed neutron counts from CRP with 6 hours' smoothing window; the red line indicates the neutron counts from COSMIC model.

And as the equation 3-7 indicates, it is anti-function of the relationship between neutron counts and soil water content, so the transform between neutron counts and soil water content conforms to an anti-function curve as Figure 5-3.

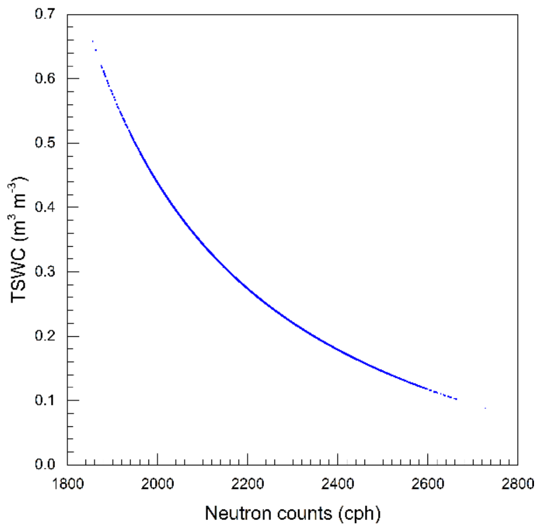

Figure 5-3 The relationship between neutron counts and soil water content

5.3. Footprint and depth of CRP

As calculating factors for CRP footprint, air pressure, air humidity and SWC fluctuates with the time, so the footprint is a not fixed value. To evaluate the approximate footprint of the CRP in the study area. The yearly average from 1st January 2016 to 10th October 2016 of these 3 factors are derived, and then footprint and depth calculated by the simplified methods (equation 3-12 and 3-16) are derived as shown in Table 5-2.

Table 5-2 Yearly results of the CRP footprints, depth and related factors.

	Unit	Maximum	Minimum	Mean	Standard deviation	Coefficient of variation (%)
Air pressure	hPa	681.83	658.47	672.46	4.07	0.60%
Air humidity	g m^{-3}	14.31	0.03	4.94	3.21	64.91%
SWC	m^3 m^{-3}	0.68	0.10	0.29	0.07	22.89%
Footprint	m	461.52	445.71	451.94	2.74	0.61%
Depth	cm	21.47	8.18	13.49	1.97	14.59%

As we can see the average footprint radius is about 452 meter, which is much bigger than the result as the reference radius (300 m) got by Marek Zreda et al. (2008). This big variation is caused by the low air pressure on the Tibetan Plateau, which means the neutron diffuse more easily.

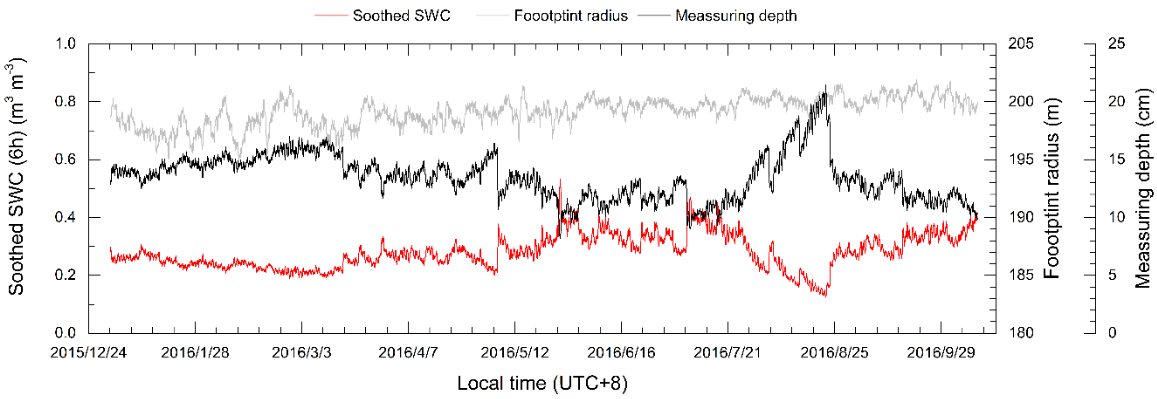

Figure 5-4 The CRP footprint and measuring depth calculated with equation 3-12 and 3-16.

Since the soil in the study area is in high moisture yearly, the depth of CRP tended to be very shallow, with only 13.5 cm average for the year. Even the highest depth in this area is 21.5 cm in a year, and the lowest depth could reach 8.2 cm.

Later on, the higher precise methods are also examined to get the footprint and depth in the study area. By checking footprint radius $R(h,\theta)$ contours in Figure 3-1 with average SWC equals 0.29 m^3 m^{-3} and average humidity 4.94 g m^{-3}, the $R(h,\theta)$ results in about 180m. After estimating the height of grass on the study area as 15 cm, and invoking the average values of air pressure, air humidity, SWC and $R(h,\theta)$ into the equations 3-13, 3-14 and 3-15, the yearly average footprint radius comes out to be 257.78 m. this radius is 43% smaller than the result calculated by the simplified method, which means the air humidity , SWC and vegetation truly lead a deeply influence on the probe footprint.

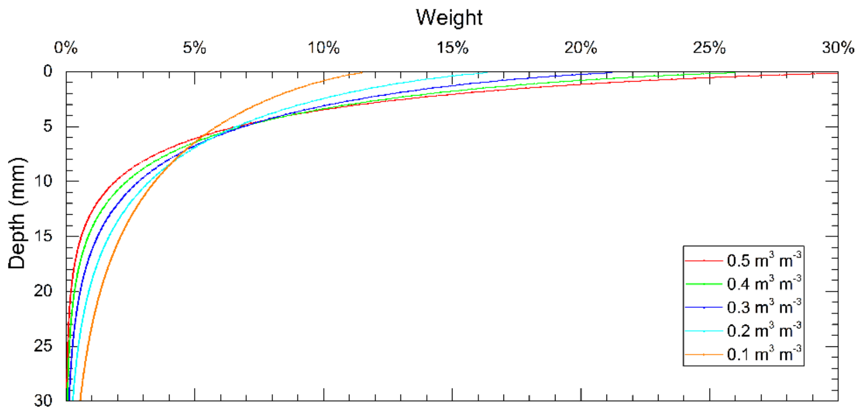

Figure 5-5 Fraction of fast neutron counts originate at each depth level (1mm) among the CRP detected neutron counts for different soil water content.

Since the COSMIC model is a model developed depends on the physic characters of neutron counts propagate, this model can illustrate the faction of neutron counts originate at each depth level (1mm) among the CRP detected neutron counts (see Figure 5-6). After cumulating the fraction of neutron counts of every depth from the ground surface (depth =0 mm), we can figure out the depth for different SWC. With the average SWC of 0.29 m^3 m^{-3}, the average measuring depth of CRP in the study area is about 12 cm by checking the cumulative fraction of fast neutron counts for different SWC in the study area (see Figure 5-6). This result is 11% smaller than the result from simplified method, because that the SWC is very high through the whole year in this area.

The 257.78 m footprint radius and 12 cm depth is more creditable than the output from the simplified method. However, these simplified methods also provide convenient approaches for obtaining the footprint and depth for the whole year (see Figure 5-4).

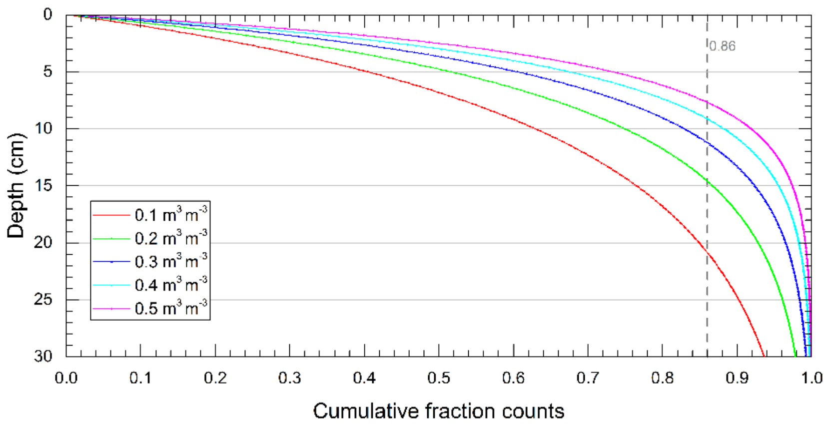

Figure 5-6 Cumulative fraction of fast neutron counts detected by CRP for different soil water content modelled by the COSMIC model . The 86% cumulative sensitivity point was normally defined as the effective depth of the sensor.

5.4. Time window for data smoothing

Since the soil water content from neutron counts is fluctuate, the time window of average moving method can affect the smoothness of the data. From the sensitive analysis result of time window (Table 5-3 and Figure 5-7), it is shown that the larger time window can result in a better correlation and tendency between the point measured soil water content and neutron counts retrieved soil water content. However, the mass balances all performed extremely well with only weakly variation (about 1%), meaning that the smoothing work does not affects much about the mass balance and the soil water content from the neutron counts can well represent the condition in reality.

Table 5-3 Sensitive analysis result of time window.

	R^2	NS	RVE
15 minutes	0.4385	-0.1305	0.89%
30 minutes	0.5487	0.2691	0.88%
45 minutes	0.5950	0.3947	0.89%
1 hour	0.6249	0.4645	0.89%
2 hours	0.6771	0.5732	0.89%
3 hours	0.6992	0.6150	0.89%
4 hours	0.7131	0.6405	0.89%
6 hours	0.7454	0.6990	0.90%
8 hours	0.7319	0.6819	0.92%
12 hours	0.7666	0.7368	0.90%
24 hours	0.7964	0.7878	0.83%

Although the larger time window trends to lead to a better correlation and tendency performance, it is not appropriate to choose the largest time window value directly, since the temporal resolution is also a significant factor for the data. Despite various objective of the data use may have different request of temporal resolution of the soil water content, 6 hours is chosen as time window for smoothing data in this study, as some other researchers did (Zhu et al., 2016). The first reason for this choice is that the influence of the time window value lager than 6 hours is very small (see Figure 5-7). And 6 hours' time window results in a peak value for both R^2 and NS. After all, this time window is chosen as a compromised result to smooth the data in this study, other than an uncontested one.

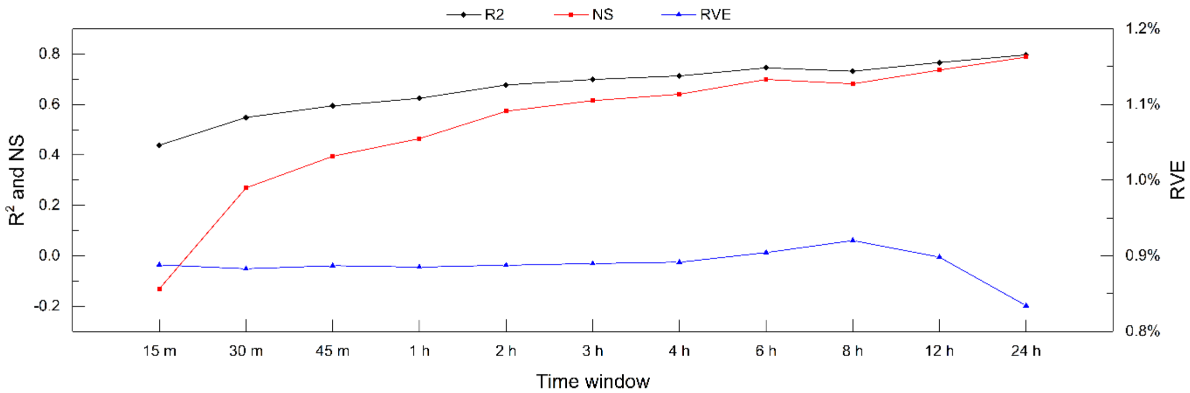

Figure 5-7 Sensitive analysis result of time window.

5.5. Validation of CRP

5.5.1. N_0 method

To test the TSWC from Neutron counts, we used the point measured LSWC from 1st May to 20th May with interval of 15 minutes. During this period, the average ST was 10 °C, and the lowest temperature was about 3.3 °C, so the total soil water is in liquid state, making the comparison between TSWC from neutron counts and point measured LSWC (depth weighted) available (see Figure 5-8).

In Figure 5-9 and Figure 5-9, the TSWC from CRP neutron counts with 15 minutes interval (blue points) fluctuates dramatically, however the smoothed 6 hours TSWC matches with the point measured LSWC very well. Particularly, a sudden rise was revealed by both smoothed TSWC and point measured LSWC between 6th of May 2016 and 7th of May 2016.

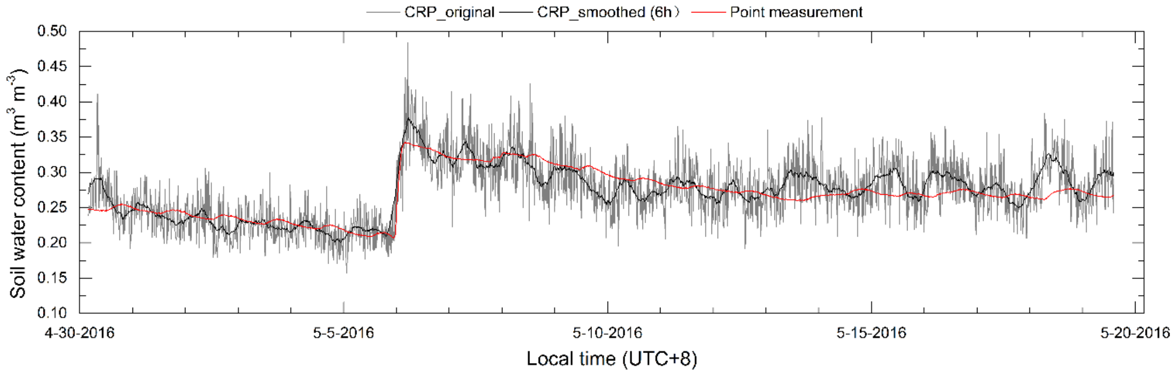

Figure 5-8 Comparison of soil water content derived from CRP neutron counts. The grey line indicates the 15 minutes soil water content from CRP neutron counts; the black line indicates the smoothed soil water content from CRP neutron counts; the red line indicates the integal soil water content (depth weighted) from point measurement.

The correlation between the original SWC (15 minutes' interval) from neutron counts and the SWC from point measurement is not obvious, because of the fluctuation of neutron counts recorded by the CRP (as Figure 5-9 (left)), while the smoothed SWC from Neutron counts is much more related to the SWC from point measurement, with R^2 results in 0.75224 (as Figure 5-9 (right)). Considering the original discrepancy between the SWC from CRP and point measurement, the R^2 being 0.75224 implies a very high correlation.

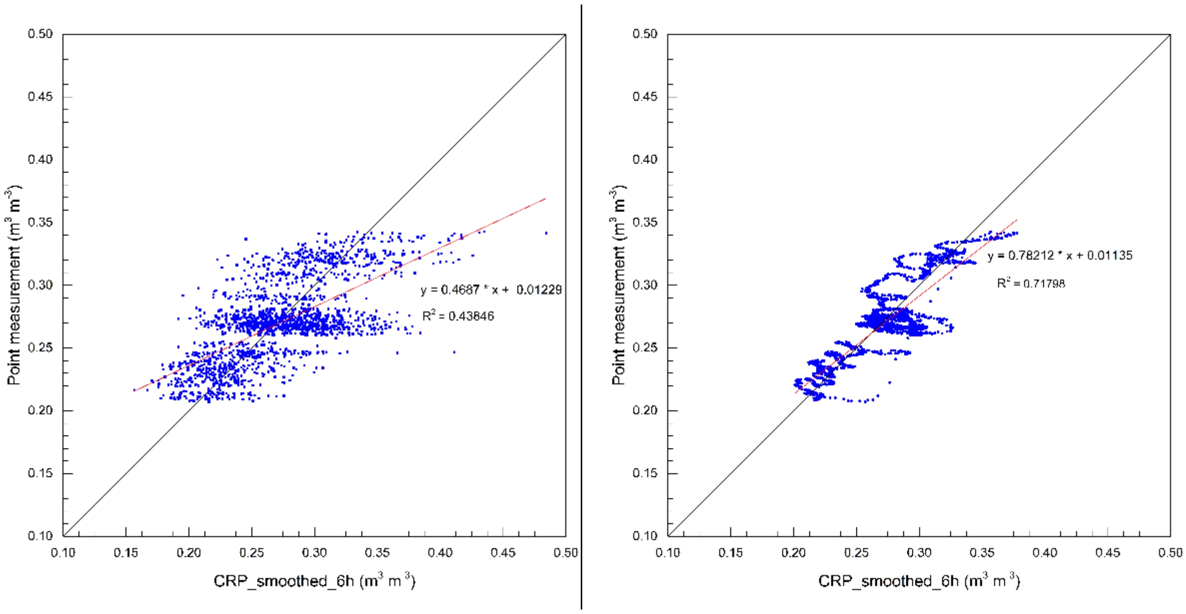

Figure 5-9 The correlation between soil water content from CRP neutron counts and average soil water content from point measurement (depth weighted). The left figure shows the correlation between 15 minutes interval soil water content from CRP neutron counts and 15 minutes soil water content from point measurement; the right figure shows the correlation between the smoothed soil water content from CRP neutron counts and the soil water content from point measurement.

5.5.2. COSMIC method

To validate the CRP, the COSMIC model is also employed, for assimilating the point measured soil water content (from 1st May to 20th May with interval of 15 minutes) to neutron counts. Then the neutron counts output from COSMIC model is compared with neutron counts with corrected CRP neutron counts during the corresponding time period (Figure 5-10).

As shown in Figure 5-10, the neutron counts from CRP with 15 minutes interval and from COSMIC model are in a reasonable agreement, especially when the neutron counts got a rapid decrease between 6th of May 2016 and 7th of May 2016. As shown in Figure 5-11, the fluctuation of neutron is violent, while the smoothed neutron counts from CRP is much more related with the neutron counts from the COSMIC model, with R square equals to 0.7522.

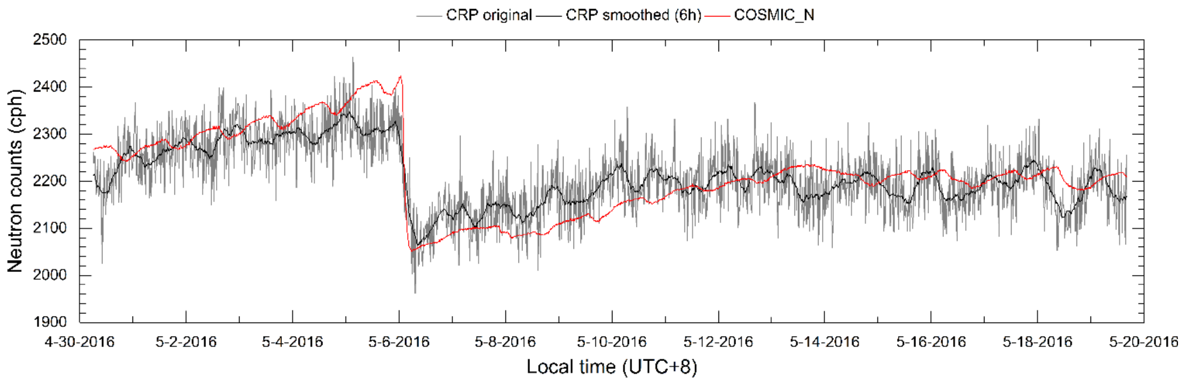

Figure 5-10 The comparison between neutron counts from CRP. The grey line indicates original neutron counts, the black line indicates the smoothed neutron counts with 6 hour time window and the red line indicates the neutron counts from COSMIC model by assimilating the point measured soil water content.

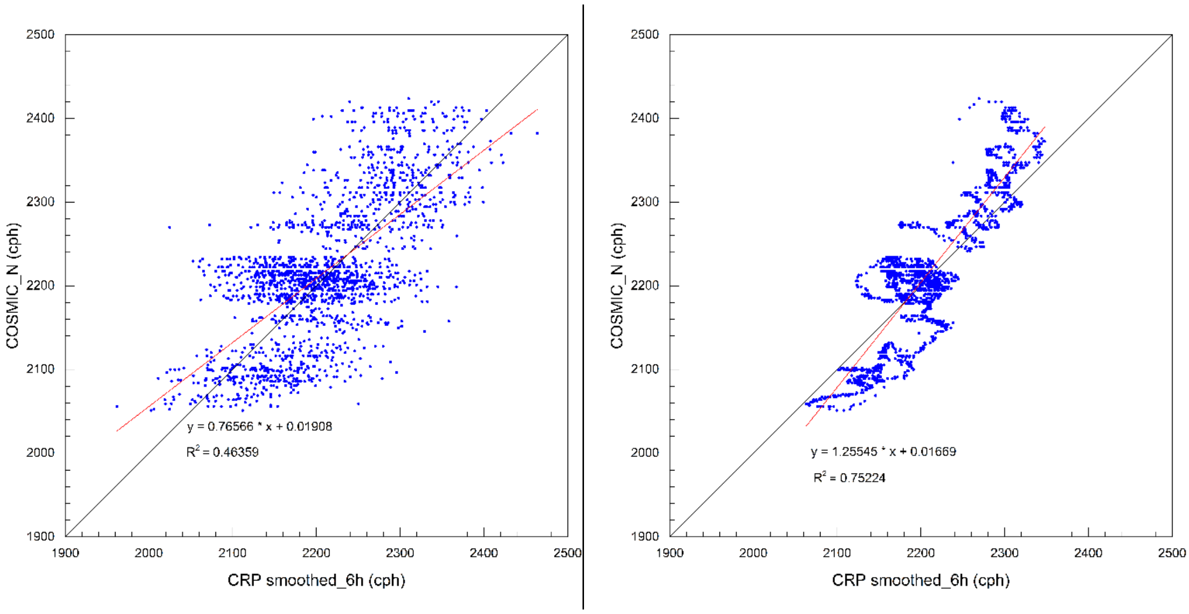

Figure 5-11 The left figure shows the correlation of neutron counts from CRP and from COSMIC model by assimilating the point measurement soil water content; the right figure shows the correlation of neutron counts from CRP (smoothed with 6 hours' time window) and from COSMIC model by assimilating the point measurement soil water content.

5.6. F-T process intepretation

5.6.1. The correlation between ST and liquid water content in frozen soil

To study the correlation between ST and LSWC in frozen soil, the point measurement data of ST/SM from 10th December 2015 to 10th February 2016 is employed, with the lowest and highest temperature being -0.2 and -11.3 °C, respectively (Figure 5-12). This data is separated into two parts, for achieving the specific objectives of correlation model calibration and validation.

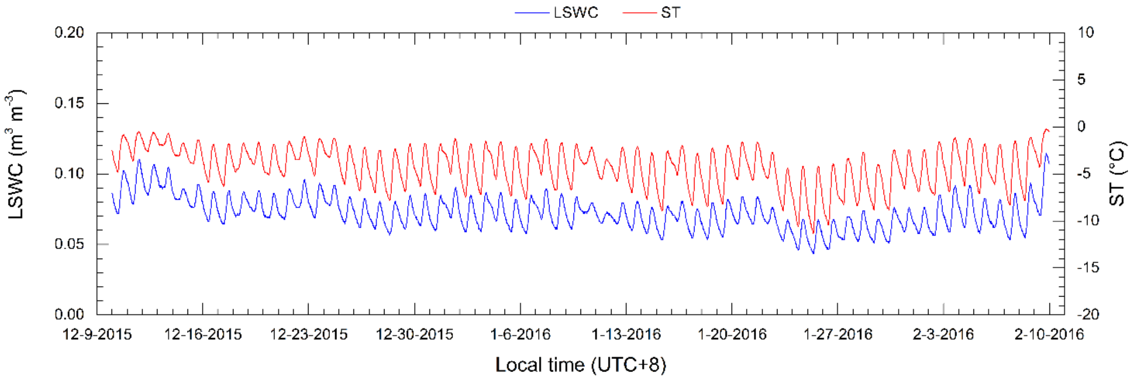

Figure 5-12 ST and LSWC measured in point measurement (this part of data is used for calibration).

From Figure 5-12, we can find that the ST fluctuates every day, and the mass of LSWC has a very obvious tendency to follow the change of the ST. To fit the correlation between ST and LSWC in frozen soil, we used five functions, in which four functions are ever adopted to simulate this correlation, and the double exponential function is newly proposed by this study (Table 5-4).

Table 5-4 The fit function, parameters and the R^2 in calibration and validaton (In these fit functions, f(x) represents the mass of the unfrozen water per unit mass of dry soil (θ_l), x represents the difference between ST and the freezing temperature (ε)).

ID	Fit function	Sources	Parameter value	R^2 in calibration	R^2 in validation
F1	f(x) = a*x^b	Anderson & Tice (1973)	a = 0.1005 b = -0.2347	0.945	0.927
F2	f(x) = a*x^b+c	Williams (1967)	a = -0.1431 b = 0.1188 c = 0.2416	0.956	0.975
F3	f(x) = a*exp(b*x) + c*exp(d*x)	This study	a = 0.04144 b = -1.42 c = 0.09476 d = -0.06417	0.961	0.982
F4	f(x) = a*exp(b*x)+c	Civan (2000)	a = 0.05793 b = -0.2896 c = 0.05437	0.9506	0.896
F5	f(x) = a*exp(b*x^2)+c	McKenzie et al. (2007)	a = 0.03485 b = -0.08342 c = 0.0628	0.917	0.937

Evaluated from the R^2 in calibration and validation in Table 5-4, these five functions works very well, especially the function proposed in this study. Evaluated from the fit result in Figure 5-13, these five functions fit the measured data extremely well on the ST value -1 to -7 °C. When ST sited out of these rang, F3 and F2 works much better than other three functions.

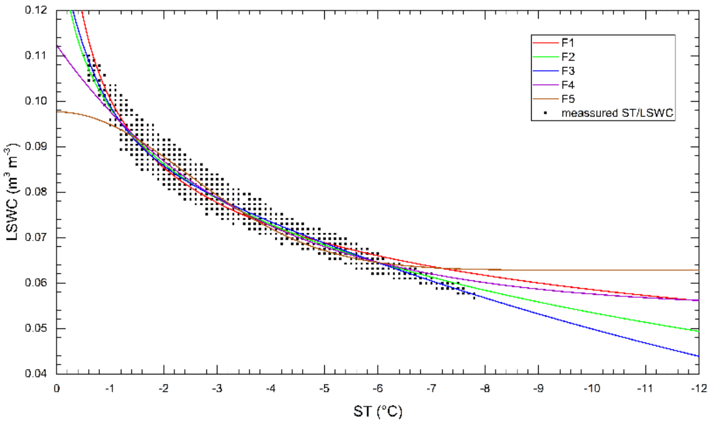

Figure 5-13 The measured ST/LSWC data and fit function curves in calibration

In the validation of the fit function, even though the R^2 result reveal that all the five function fit with the measured ST/LSWC very well (Table 5-4), the fit result in Figure 5-14 represent that all the five function have the tendency to overestimate the LSWC. When the ST value stay above -1°C, the result from F5 deflect strongly, while the other four functions' results are reasonable. When the ST value stay below -7°C, F3 and F2 are still valid, but other three functions would exaggerate the LSWC result.

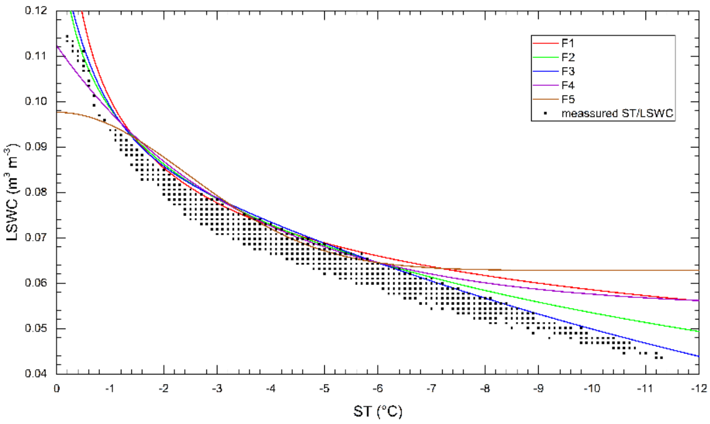

Figure 5-14 The measured data and fit function curves in validation

In the calibration and validation of the functions to model the correlation between ST and LSWC in frozen soil, it present that the function F3 which proposed in this study can behave better than other empirical function. Besides the good performance in ST value range (-1, -7), the double exponential function F3 can also simulate the correlation well at the ST near 0 °C and below 10 °C.

5.6.2. SIC from in-situ measured LSWC and CRP

According to equation 3-23, it is available to get the SIC, by invoking average TSWC from CRP neutron counts and LSWC from point measurement. As shown in Figure 5-15, the LSWC fluctuates along with the ST, and lower ST trends to result in less liquid soil water. Although having an inverse changing trend with the ST, the SIC tend to follow the mass of TSWC. This character of SIC is obviously expressed in the situation of 13th January 2016, when the SIC followed the increment of TSWC, the LSWC did not respond.

In January 2016, the average percentage of LSWC and SIC to TSWC in the study area is about 30% and 70%, respectively. Under the extremely low ST (about -10 °C), the percentage of LSWC reaches the low value of 20%.

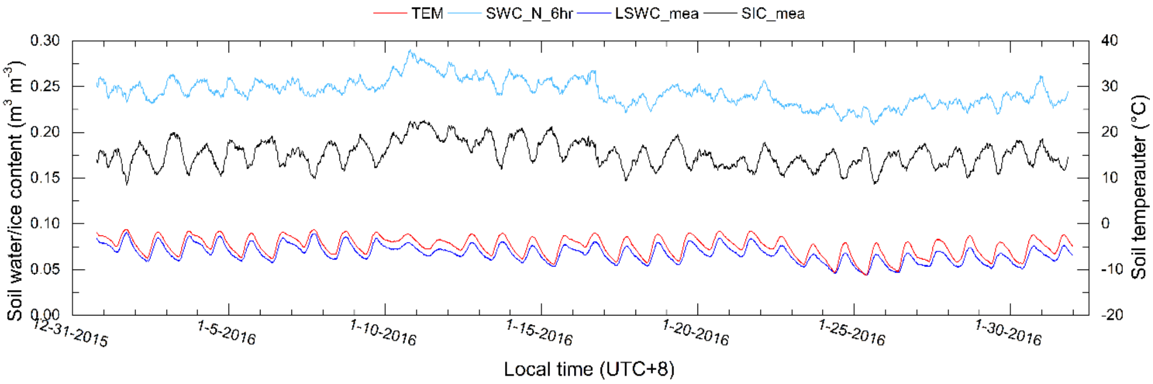

Figure 5-15 Derivation of SIC from LSWC. The blue and red line indicates the LSWC and ST from point measurement, respectively; the light blue line indicates the smoothed (6 hours) TSWC measured by the CRP, and the grey line indicates the SIC derived from measured LSWC.

5.6.3. SIC from ST and CRP

After the correlation between ST and LSWC in frozen soil is clear, it is available to derive the SIC from the CRP data and ST directly. With the help of the double exponential function shown in Table 5-4, the LSWC is simulated for the calculation for SIC (Figure 5-16). With this correlation, the calculation of SIC would be much fast and convenient, and the applications of CRP would be promoted.

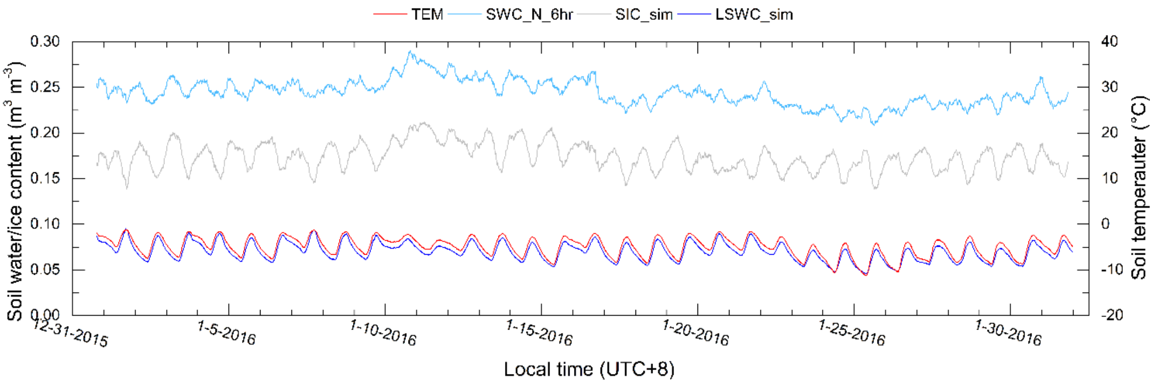

Figure 5-16 Derivation of SIC from ST. The blue and red line indicates the LSWC and ST from point measurement, respectively; the light blue line indicates the smoothed (6 hours) TSWC measured by the CRP, and the grey line indicates the SIC derived from ST.

5.6.4. Comparison of two SICs

By comparing the two kinds of SIC, we can find the correlation between ST and LSWC in frozen soil is extremely high (Figure 5-17). By comparing he two kinds of SIC during the first month of 2016, it is found that the biggest deviation between them is 4.76% and the R^2 for this whole month is 0.99472. It is notable that the correlation between ST and LSWC was derived purely from the in-situ measurement, in a way to determine the SIC. In order to validate the results further, the in-door experiment on measuring the SIC needs to be implemented. Nevertheless, this lab determination of SIC will not be carried out for this study, due to the time limitation.

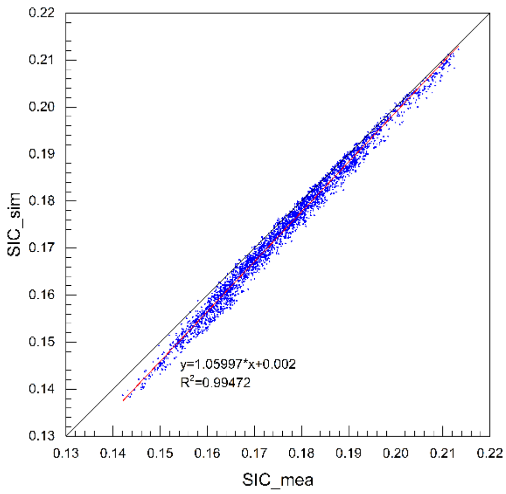

Figure 5-17 The correlation between SICs calculated from LSWC and ST.

6. DISCUSSION

6.1. Errors in CRP calibration

The intention of CRP calibration is to build the contraction between the CRP neutron counts and the SWC in the field. To achieve this field work is executed to measure the SWC in field by oven drying method. Although this procedure finished conveniently, some undesirable errors are still included in the calibration.

1. Unwelcome weather condition

The SWC measured by the CRP is the total soil water below the probe, while the soil sampling only measured the water in the soil (without lattice water and organic water). Thus the any water stay under the CRP machine could lead to errors to the calculation. Unfortunately, when proceeding the soil sampling, an undesirable heavy rain was appeared, resulting in water persistence on the standing biomass. To depress the influence of rainy weather, a value of 0.02 (m^3 m^{-3}) was added to the soil measured SWC in calibration calculation.

2. Irregularity of soil sampling sites

As mentioned in the field work plan (Figure 4-1), the soil sampling sites should be regular, for the purpose of improving the accuracy of the mean SWC. However, it was not realistic to carry out the plan in the field because of the complicate condition and the proprietorship of the farmland. The final sampling sites result in an irregular shape as Figure 4-2, which would lead to a deviation of the mean SWC in the field work.

3. Depth and distance not weighted

By detecting the neutron counts, the CRP measured average SWC is related to the soil depth and distance to the probe, and the soil water located closer to the CRP or at shallower depth could get a higher weight of the final average SWC. However, to simplify the calculation, the average SWC for calibrating the CRP is in arithmetic average of all the soil samplings, which is different with the average SWC from CRP. After all, it is possible to give a weight to every soil samples before the CRP measuring depth and footprint radius determined.

6.2. Discrepancies between CRP detected SWC and point measurement

In this study, the SWC from CRP and from point measurement during non-frozen season is treated as highly correlated to for further analysis. Although the homogeneous grassland can drive down the offsets between them and the result also showed these two sets of data were highly correlated (R^2=0.7454 after smoothing with 6 hours' time window for CRP data), there are some reasons can explain the discrepancy between these two sets of data:

1. Distance between two measuring area.

The CRP footprint radius was figured out to be about 257.78 m in the study area, however the point measurement site is located at south-west direction of CRP about 4000 meters away. A closer distance between the measurement sites could depress this offset according to the Tobler's First Law of Geography: all attribute values on a geographic surface are related to each other, but closer values are more strongly related than are more distant ones (Tobler, 1970). After all, a point measurement located within the CRP is the prime option if available.

2. Measuring scale

By detecting the neutron counts, CRP could measuring the average SWC at its footprint. Due to the limitation of the field condition, this study can only acquire the SWC from one site. To improve the accuracy of calculation, a distributed sensor network is recommended for calculating the mean SWC in the footprint of CRP (Trenton E. Franz, Zreda, Rosolem, et al., 2012; Jiao, Zhu, & Du, 2014). Furthermore, with distributed sensor network, the average SWC calculation could take the distance weight into consideration to improve the accuracy.

6.3. Is the LSWC independent to the TSWC in frozen ground?

Even though the high correlation between the ST and LSWC and the low correlation between ST and TSWC implies that the correlation between LSWC and TSWC could not be strong, the question whether the LSWC independent to the TSWC keeps being controversial. Many researchers have claimed that their independence according to experimentation and/or thermodynamic theory (Fisher, 1924; Low, Hoekstra, & Anderson, 1968; Spaans & Baker, 1996). However, some other researchers found that the in-situ results indicated independence between LSWC and TSWC (Yong, 1965).

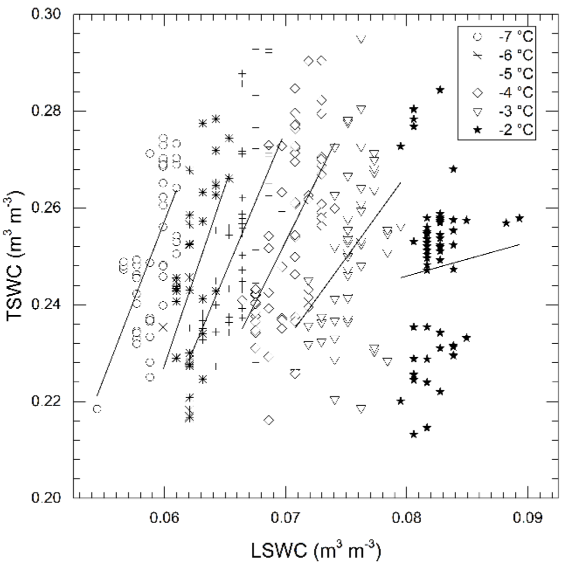

Tem	Function	R2
-2	y=0.69781x+1.29319	0.00517
-3	y=3.44797x+1.15709	0.14350
-4	y=5.02076x+0.85340	0.34747
-5	y=5.94977x+1.05263	0.35128
-6	y=7.39031x+1.78505	0.31085
-7	y=6.48105x+1.18762	0.40918

Figure 6-1 The correlation between TSWC and LSWC at specific temperatures. The straight lines indicate the fitting lines for the points at specific temperatures and the table on the right shows the fitting function and R^2.

To test the LSWC's independence to TSWC, the relationship between TSWC and LSWC at specific temperatures (-2, -3, -4, -5, -6, -7 °C) is presented in Figure 6-1. As the result shown, the LSWC has a tendency of increasing when the TSWC increases, especially at low ST. That means the LSWC is truly dependent to the TSWC in our study. For the further study, the dependence between TSWC and LSWC should be included for a better simulation of FT process.

6.4. Does the lag of FT process to ST in frozen ground exist?

Two conceptions have been generally accepted by researchers sine decades ago: 1. the LSWC can be expressed as a function of ST; 2. the FT process in the frozen soil undergoes a gradual phase change (Duwayne M. Anderson, Tice, & McKim, 1973; Civan, 2000; Inaba, 1983; Kurylyk & Watanabe, 2013). For the first conception, it is based on the principle that the ST and LSWC are corresponded to each other, while for the second conception, it is not considered problem that weather the state of ST and the state of the LSWC should be in synchronization. They are not related the lag of the FT process to ST in frozen ground, for models simulating the correlation between ST and LSWC until now.

Although the newly adopted correlation model, the double exponential function, performs extremely well in this study, it is still easy to find that: for the same temperature, the LSWC could be various as shown in the Figure 5-13 or Figure 5-14. Normally, in the reported studies this discordance were mostly neglected as observational error and assumed an instantaneous phase change in FT process for computational convenience (McKenzie et al., 2007; Norum & Jame, 1972; Xia & Shufen, 2011; Kozlowski & Nartowska, 2013).

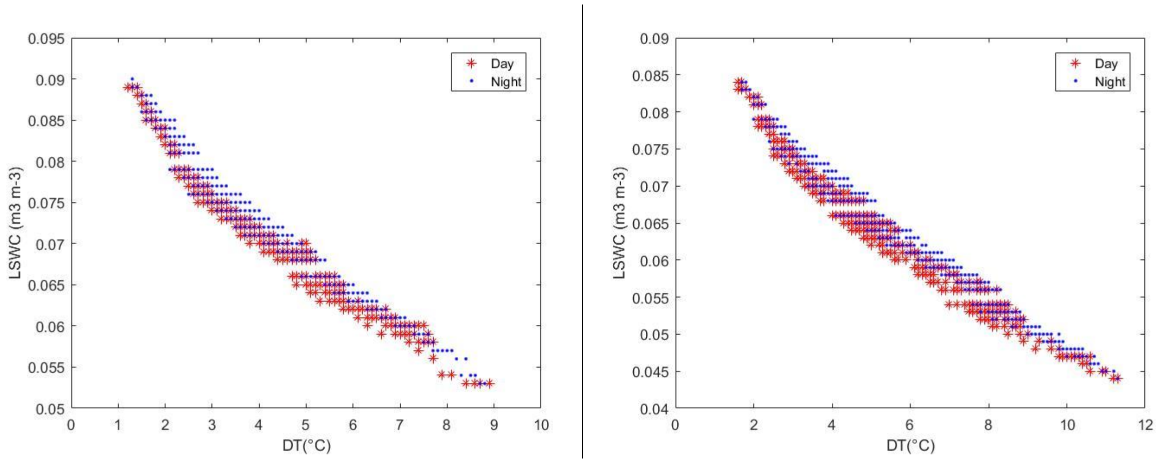

Figure 6-2 The present of ST/LSWC data by point measurement after separated into daytime and night-time two parts (The red points indicates the daytime data and the blue points indicates the night time data; DT represent the difference between ST and the freezing temperature). The left figure shows the result of the first 15 days in January 2016 and the right figure shows the result of the left 15 days in January 2016.

In order to explore the reason of this deviation, the ST/LSWC data were separated into two parts, the temperature increasing part and temperature decreasing part (or simply called daytime part and night-time part). As shown in Figure 6-2, the daytime data and night-time data have a tendency to separate into 2 levels. This tendency implies that the LSWC in freezing process tend to be more than the thawing process for the same ST. Although this phenomenon cannot prove the exitance of the lag in FT process, it is in accordance with the existence of the FT process lag to ST.

Then the LSWC at five different ST (-3, -4, -5, -6, -7 °C) was combined with the change of ST from fixed intervals (15 minutes, 30 minutes, 45 minuters, 1 hour, 2hours and 3 hours) ago, for removing the influence of the ST variation. As shown in Figure 6-3, For different temperatures and intervals, the mass of LSWC all present tend to be negtive correlation to the difference of the ST. That means the faster the ST increases, the less the LSW tend to be, and vive verse.

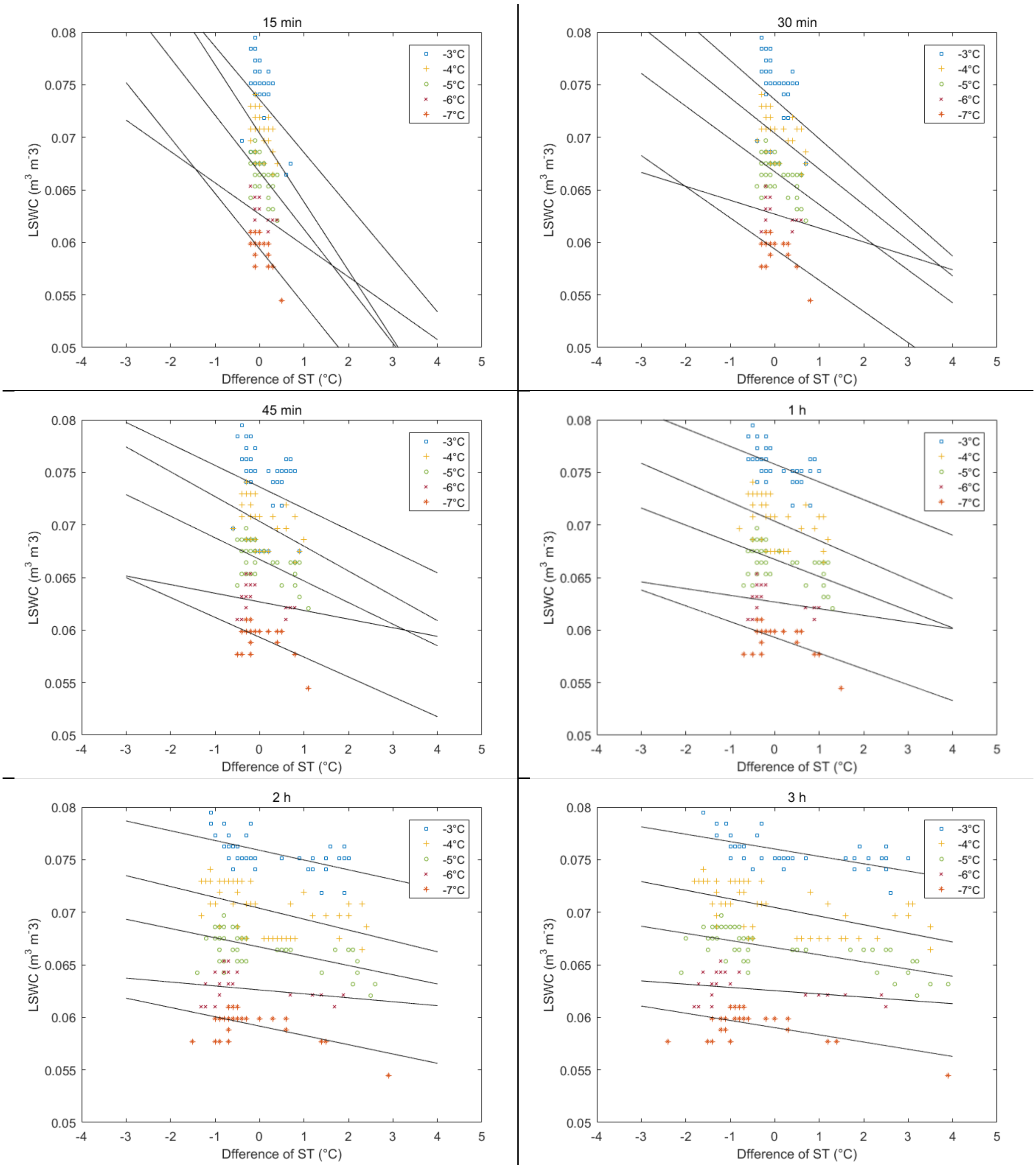

Figure 6-3 The relationship between difference of ST and LSWC at five specific temperature (-3, -4, -5, -6, -7 °C). The five straight lines in each picture are the fit lines to the points for specific temperature.

To help verify this point furtherly, Two sets of difference data is calculated: 1. the difference between measured LSWC and simulated LSWC from double correlation model; 2. the difference between the ST at specific time and the ST 3 hours ago. The difference between LSWC is related to describe the lag of FT to ST processes and the difference of ST is related to the rate of ST change. As shown in Figure 6-4, this FT lag is highly correlated with the ST change speed, with the R^2 equals to 0.8753. When the ST is increasing, (difference of T is positive in Figure 6-4) the simulated LSWC is normally underestimated compared to the in-situ measured result, since the simulation did not take the lag in to consideration.

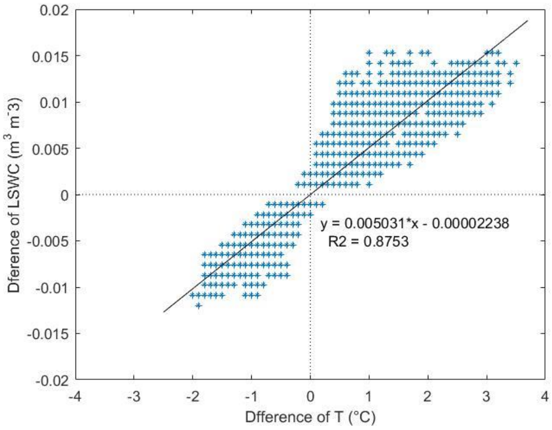

Figure 6-4 The Difference of LSWC and ST result.

From the results above, we can find that the correlation of ST and LSWC is not exactly corresponded, and there is a lag of FT process to ST in frozen ground As a result, to simulating the correlation between ST and LSWC, the lag of FT process to the ST should be included for higher accuracy. Although recognised the lag of FT process to ST, this study still remained to use the double exponential correlation model directly to simulate the LSWC, because of the time limitation.

6.5. Potential physic meaning in the double exponential function

For the correlation function proposed to describe the ST and LSWC relationship, former researchers always explain the potential physical principles contained. Normally, researchers treat the SWC absorbed by the soil grains as a constant (Civan, 2000; Kurylyk & Watanabe, 2013; McKenzie, Voss, & Siegel, 2007b). This assumption is for an approximation but not exactly correct.

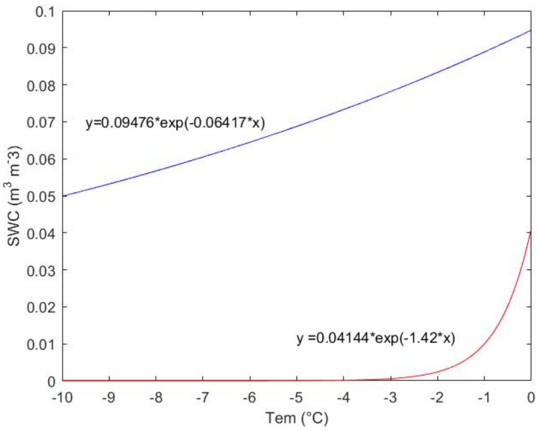

Figure 6-5 The exponential function used in the correlation model.

To explain the double exponential function, we would like to classify the water into three parts: 1. gravity water, which is sensitive to the freezing points. This part of soil water is assumed to be entirely frozen in the soil water; 2. the capillary water, which is also affected by the soil grains but much feebly, can be described by one of the double function (y =0.04144*exp(-1.42*x)) (red curve in Figure 6-5); 3. the soil hygroscopic water, which is drew by the soil grains tightly, can be described by the other function in the double function model (y=0.09476*exp(-0.06417*x)) (blue curve in Figure 6-5). According to the parameters in this two functions, the soil film water is 0.04144 (m^3m^{-3}), while the soil hygroscopic water is 0.09476 (m^3 m^{-3}). And the function about soil hygroscopic water is insensitive to the ST. Especially, when the ST is very low, this part of LSWC is tend to be invariable, coinciding with the point that absorbed soil water is a constant.

After all, the explanation here for the correlation functions is just an assumption, and its authenticity is still need to be proved. Furthermore, an accurate description of the reality the range of parameters a and b should be defined before the fitting.

7. CONCLUSION

Detecting cosmic-ray neutrons is a new method for measuring mean SWC at hectometre scales and can compensate for scales differences between conventional point measurements and remote sensing retrieval. It has the advantages of nonintrusive, continuous observation with high time resolution and represents a new approach for SWC studies.

A cosmic-ray neutrons probe was installed on the northern Tibetan Plateau for measuring the mean SWC during the year of 2016. To employ this probe, a field work is executed for calibrating it. With the soil sampling result, both N_0 method and COSMIC model method were adopted to calibrate the CRP, and two calibration method resulted in two N_0 value very similar, with only 0.5395% of the deviation. After the calibration, the first validation the is achieved with N_0 method by comparing the SWC data derived from CRP with the SWC data from point measuring method, which revealed a satisfied result. While another validation is achieved by comparing the neutron counts from CRP and the neutron counts simulated with COSMIC model from point measurement data, which revealed a satisfied result as well. The R square of two validation method are both about 75%. As the fluctuation of the original CRP data, the time window for smoothing the data is tested, and 6 hours was chosen as the time window in this study.

The point measurement system with SM/ST probes was set near the CRP to measure the SWC and temperature at various soil depths. To study the FT process in frozen ground, the ST/LSWC data is employed to pick a good model for simulating the correlation between ST and LSWC below freezing temperature. The double exponential function is proposed to simulate the LSWC with ST, and the result presents that this function run well.

This study also measured the SIC during the frozen period of ground with two methods: from the LSWC by point measurement and from ST by simulation. These two results matched with each other very well. later, the Errors in CRP calibration, discrepancies between CRP detected SWC and point measure, the lag of FT process to ST change in frozen ground and the potential meaning of the double exponential model is discussed at the end.

The study results proved that the cosmic-ray method was well applicable in frozen ground, the ST is highly correlated with the LSWC and the SIC derived from the neutron counts and ST is in high accuracy when compared with SIC from the neutron counts and LSWC from point measurement. This study introduce the CRP to help the detection of the FT process over frozen ground, laying a scientific basis for the application of the CRP for monitoring SWC in high and cold areas and represents a new approach for the study of SWC and SIC on the Tibetan Plateau.

LIST OF REFERENCES

A. Wahbi, G. D. H. (2015). *Cosmic Ray Neutron Probe : Use , Calibration and Validation*.

Anderson, D. M., & Tice, A. R. (1973). The unfrozen interfacial phase in frozen soil water systems. In A. Hadas, D. Swartzendruber, P. E. Rijtema, M. Fuchs, & B. Yaron (Eds.), *Physical Aspects of Soil Water and Salts in Ecosystems* (pp. 107–124). Berlin, Heidelberg: Springer Berlin Heidelberg. https://doi.org/10.1007/978-3-642-65523-4_12

Anderson, D. M., Tice, A. R., & McKim, H. L. (1973). The unfrozen water and the apparent specific heat capacity of frozen soils. *Proceedings of the Second International Conference on Permafrost*, (4), 289–295. Retrieved from http://books.google.com/books?hl=en&lr=&id=M4SvF9Qax7EC&oi=fnd&pg=PA289&dq=The+Unfrozen+Water+and+the+Apparent+Specific+Heat+Capacity+of+Frozen+Soils&ots=gqCuiMEERT&sig=xPkvkYEdPywlitBsT_rTa0fRRI0

Applications, F. T., Mizoguchi, M., Lundin, L., & Genuchten, M. T. Van. (2004). Water Flow and Heat Transport in Frozen Soil : Numerical Solution. *Vadose Zone Journal*, *3*(2), 693–704. https://doi.org/10.2113/3.2.693

ASTM D2216-10. (2010). Standard Test Methods for Laboratory Determination of Water (Moisture) Content of Soil and Rock by Mass, 7. https://doi.org/10.1520/D2216-10

Belcher, D. J., Cuykendall, T. R., & Sack, H. S. (1950). The measurement of soil moisture and density by neutron and gamma ray scattering. *Technical Development and Evaluation Center*, 20.

Bogena, H. R., Huisman, J. A., Baatz, R., Hendricks Franssen, H. J., & Vereecken, H. (2013). Accuracy of the cosmic-ray soil water content probe in humid forest ecosystems: The worst case scenario. *Water Resources Research*, *49*(9), 5778–5791. https://doi.org/10.1002/wrcr.20463

Bronfenbrener, L., & Bronfenbrener, R. (2012). A temperature behavior of frozen soils: Field experiments and numerical solution. *Cold Regions Science and Technology*, *79–80*, 84–91. https://doi.org/10.1016/j.coldregions.2012.03.005

Brooks, R. H., & Corey, A. T. (1964). Properties of Porous Media Affecting Fluid Flow. *ASCE Journal of the Irrigation and Drainage Division*, *92*(2), 61–90.

Civan, F. (2000). Unfrozen Water in Freezing and Thawing Soils: Kinetics and Correlation. *American Society of Civil Engineers*, *14*(3), 146–156. https://doi.org/doi.org/10.1061/(ASCE)0887-381X(2000)14:3(146)

D'Odorico, P., Caylor, K., Okin, G. S., & Scanlon, T. M. (2007). On soil moisture-vegetation feedbacks and their possible effects on the dynamics of dryland ecosystems. *Journal of Geophysical Research: Biogeosciences*, *112*(4), 1–10. https://doi.org/10.1029/2006JG000379

Desilets, D., & Zreda, M. (2001). On scaling cosmogenic nuclide production rates for altitude and latitude using cosmic-ray measurements. *Earth and Planetary Science Letters*, *193*(1–2), 213–225. https://doi.org/10.1016/S0012-821X(01)00477-0

Desilets, D., & Zreda, M. (2003). Spatial and temporal distribution of secondary cosmic-ray nucleon intensities and applications to in situ cosmogenic dating. *Earth and Planetary Science Letters*, *206*(1–2), 21–42. https://doi.org/10.1016/S0012-821X(02)01088-9

Desilets, D., & Zreda, M. (2013). Footprint diameter for a cosmic-ray soil moisture probe: Theory and Monte Carlo simulations. *Water Resources Research*, *49*(6), 3566–3575. https://doi.org/10.1002/wrcr.20187

Desilets, D., Zreda, M., & Ferré, T. P. A. (2010). Nature's neutron probe: Land surface hydrology at an elusive scale with cosmic rays. *Water Resources Research*, *46*(11), n/a-n/a. https://doi.org/10.1029/2009WR008726

Evan, S. (1965). Dielectric properties of ice and snow-a review. *Journal of Glaciology*, *5*(42), 773–792. https://doi.org/10.3198/1965JoG5-42-773-792

Excel. (n.d.). RSQ Function. Retrieved from http://office.microsoft.com/en-gb/excel-help/rsq-function-HP010342863.aspx

Fisher, E. A. (1924). The freezing of water in capillary systems. A critical discussion. *Journal of Physical Chemistry*, *28*(4), 360–367. https://doi.org/10.1021/j150238a006

Franz, T. E., Wahbi, A., Vreugdenhil, M., Weltin, G., Heng, L., Oismueller, M., … Desilets, D. (2016). Using cosmic-ray neutron probes to monitor landscape scale soil water content in mixed land use agricultural systems. *Applied and Environmental Soil Science*, *2016*, 1–11. https://doi.org/10.1155/2016/4323742

Franz, T. E., Zreda, M., Ferre, T. P. A., Rosolem, R., Zweck, C., Stillman, S., … Shuttleworth, W. J. (2012). Measurement depth of the cosmic ray soil moisture probe affected by hydrogen from various sources. *Water Resources Research*, *48*(8), 1–9. https://doi.org/10.1029/2012WR011871

Franz, T. E., Zreda, M., Rosolem, R., & Ferre, T. P. a. (2012). Field Validation of a Cosmic-Ray Neutron Sensor Using a Distributed Sensor Network. *Vadose Zone Journal*, *11*(4), 1–10. https://doi.org/10.2136/vzj2012.0046

Franz, T. E., Zreda, M., Rosolem, R., & Ferre, T. P. A. (2013). A universal calibration function for determination of soil moisture with cosmic-ray neutrons. *Hydrology and Earth System Sciences*, *17*(2), 453–460. https://doi.org/10.5194/hess-17-453-2013

Gardner, W., & Kirkham, D. (1952). Determination Of Soil Moisture By Neutron Scattering. *Soil Science*, *73*(5), 391–401. https://doi.org/10.1097/00010694-195205000-00007

Han, X., Franssen, H. J. H., Rosolem, R., Jin, R., Li, X., & Vereecken, H. (2015). Correction of systematic model forcing bias of CLM using assimilation of cosmic-ray Neutrons and land surface temperature: A study in the Heihe Catchment, China. *Hydrology and Earth System Sciences*, *19*(1), 615–629. https://doi.org/10.5194/hess-19-615-2015

Han, X., Hendricks Franssen, H. J., Jiménez Bello, M. Á., Rosolem, R., Bogena, H., Alzamora, F. M., … Vereecken, H. (2016). Simultaneous soil moisture and properties estimation for a drip irrigated field by assimilating cosmic-ray neutron intensity. *Journal of Hydrology*, *539*, 611–624. https://doi.org/10.1016/j.jhydrol.2016.05.050

Han, X., Jin, R., Li, X., & Wang, S. (2014). Soil moisture estimation using cosmic-ray soil moisture sensing at heterogeneous farmland. *IEEE Geoscience and Remote Sensing Letters*, *11*(9), 1659–1663. https://doi.org/10.1109/LGRS.2014.2314535

Heidbuchel, I., Guntner, A., & Blume, T. (2016). Use of cosmic-ray neutron sensors for soil moisture monitoring in forests. *Hydrology and Earth System Sciences*, *20*(3), 1269–1288. https://doi.org/10.5194/hess-20-1269-2016

Inaba, H. (1983). Heat transfer behavior of frozen soils. *Trans. ASME: J. Heat Transfer*, *105*(3), 680–683. https://doi.org/10.1115/1.3245646

Jackson, R. D. (1973). Diurnal changes in soil water content during drying. In *Field soil water regime* (pp. 37–55). https://doi.org/10.2136/sssaspecpub5.c3

Jiang, J. H., & Wu, D. L. (2004). Ice and water permittivities for millimeter and sub-millimeter remote sensing applications. *Atmospheric Science Letters*, *5*(7), 146–151. https://doi.org/10.1002/asl.77

Jiao, Q., Zhu, Z., & Du, F. (2014). Theory and application of measuring mesoscale soil moisture by cosmic-ray fast neutron probe. *IOP Conference Series: Earth and Environmental Science*, *17*, 12147. https://doi.org/10.1088/1755-1315/17/1/012147

Kim, Y., Kimball, J. S., McDonald, K. C., & Glassy, J. (2011). Developing a global data record of daily landscape freeze/thaw status using satellite passive microwave remote sensing. *IEEE Transactions on Geoscience and Remote Sensing*, *49*(3), 949–960. https://doi.org/10.1109/TGRS.2010.2070515

Kim, Y., Kimball, J. S., Zhang, K., & McDonald, K. C. (2012). Satellite detection of increasing Northern Hemisphere non-frozen seasons from 1979 to 2008: Implications for regional vegetation growth. *Remote Sensing of Environment*, *121*, 472–487. https://doi.org/10.1016/j.rse.2012.02.014

Kodama, M., Nakai, K., Kawasaki, S., & Wada, M. (1979). An application of cosmic-ray neutron measurements to the determination of the snow-water equivalent. *Journal of Hydrology*, *41*(1–2), 85–92. https://doi.org/10.1016/0022-1694(79)90107-0

Köhli, M., Schrön, M., Zreda, M., Schmidt, U., Dietrich, P., & Zacharias, S. (2015). Footprint characteristics revised for field-scale soil moisture monitoring with cosmic-ray neutrons. *Water Resources Research*, *51*(7), 5772–5790. https://doi.org/10.1002/2015WR017169

Kozlowski, T. (2007). A semi-empirical model for phase composition of water in clay-water systems. *Cold Regions Science and Technology*, *49*(3), 226–236. https://doi.org/10.1016/j.coldregions.2007.03.013

Kozlowski, T., & Nartowska, E. (2013). Unfrozen Water Content in Representative Bentonites of Different Origin Subjected to Cyclic Freezing and Thawing. *Vadose Zone Journal*, *12*, doi:10.2136/vzj2012.0057. https://doi.org/10.2136/vzj2012.0057

Kurylyk, B. L., & Watanabe, K. (2013). The mathematical representation of freezing and thawing processes in variably-saturated, non-deformable soils. *Advances in Water Resources*, *60*, 160–177. https://doi.org/10.1016/j.advwatres.2013.07.016

Low, P. F., Hoekstra, P., & Anderson, D. M. (1968). Some Thermodynamic Relationships for Soils at or Below the Freezing Point: 2. Effects of Temperature and Pressure on Unfrozen Soil Water. *Water Resources Research*, *4*(3), 541–544. https://doi.org/10.1029/WR004i003p00541

McHenry, J. R. (1963). Theory and application of neutron scattering in the measurement of soil moisture. *Soil Science*, *95*(5), 294–307.

McKenzie, J. M., Voss, C. I., & Siegel, D. I. (2007a). Groundwater flow with energy transport and water-ice phase change: Numerical simulations, benchmarks, and application to freezing in peat bogs. *Advances in Water Resources*, *30*(4), 966–983. https://doi.org/10.1016/j.advwatres.2006.08.008

McKenzie, J. M., Voss, C. I., & Siegel, D. I. (2007b). Groundwater flow with energy transport and water-ice phase change: Numerical simulations, benchmarks, and application to freezing in peat bogs. *Advances in Water Resources*, *30*(4), 966–983. https://doi.org/10.1016/j.advwatres.2006.08.008

Musa, A., Ya, L., Anzhi, W., & Cunyang, N. (2016). Characteristics of soil freeze-thaw cycles and their effects on water enrichment in the rhizosphere. *Geoderma*, *264*, 132–139. https://doi.org/10.1016/j.geoderma.2015.10.008

Nash, J. E., & Sutcliffe, J. V. (1970). River flow forecasting through conceptual models part I - A discussion of principles. *Journal of Hydrology*, *10*(3), 282–290. https://doi.org/10.1016/0022-1694(70)90255-6

Norum, D. I., & Jame, Y. W. (1972). Phase Composition of a Partially Frozen Soil. *Amarican Geophysical Union*, (11), 17.

O'Kelly, B. C. (2004). Accurate Determination of Moisture Content of Organic Soils Using the Oven Drying Method. *Drying Technology*, *22*(7), 1767–1776. https://doi.org/10.1081/DRT-200025642

Pelowitz, D. B. (2011). MCNPX User's Manual. In *Cell* (pp. 1–76). https://doi.org/LA-CP-05-0369

Podest, E., McDonald, K. C., & Kimball, J. S. (2014). Multi sensor microwave sensitivity to freeze thaw dynamics across a complex boreal landscape. *IEEE Transactions on Geoscience and Remote Sensing*, *(In-press)*(11), 6818–6828.

Romanovsky, V. E., & Osterkamp, T. E. (2000). Effects of unfrozen water on heat and mass transport processes in the active layer and permafrost. *Permafrost and Periglacial Processes*, *11*(3), 219–239. https://doi.org/10.1002/1099-1530(200007/09)11:3<219::AID-PPP352>3.0.CO;2-7

Rosolem, R., Shuttleworth, W. J., Zreda, M., Franz, T. E., Zeng, X., & Kurc, S. a. (2013). The Effect of Atmospheric Water Vapor on Neutron Count in the Cosmic-Ray Soil Moisture Observing System. *Journal of Hydrometeorology*, *14*(5), 1659–1671. https://doi.org/10.1175/JHM-D-12-0120.1

Shuttleworth, J., Rosolem, R., Zreda, M., & Franz, T. (2013). The COsmic-ray Soil Moisture Interaction Code (COSMIC) for use in data assimilation. *Hydrology and Earth System Sciences*, *17*(8), 3205–3217. https://doi.org/10.5194/hess-17-3205-2013

Spaans, E. J. A., & Baker, J. M. (1996). The soil freezing characteristic: Its measurement and similarity to the soil moisture characteristic. *Soil Science Society of America Journal*, *60*(1), 13. https://doi.org/10.2136/sssaj1996.03615995006000010005x

Stone, J. F., Kirkham, D., & Read, A. A. (1955). Soil Moisture Determination by a Portable Neutron Scattering Moisture Meter. *Soil Science Society of America Journal*, *19*(4), 419–423. https://doi.org/10.2136/sssaj1955.03615995001900040007x

Su, Z., Wen, J., Dente, L., Van Der Velde, R., Wang, L., Ma, Y., … Hu, Z. (2011). The tibetan plateau observatory of plateau scale soil moisture and soil temperature (Tibet-Obs) for quantifying uncertainties in coarse resolution satellite and model products. *Hydrology and Earth System Sciences*, *15*(7), 2303–2316. https://doi.org/10.5194/hess-15-2303-2011

Tobler, W. R. (1970). A Computer Movie Simulating Urban Growth in the Detroit Region. *Economic Geography*, *46*(2), 234–240. https://doi.org/10.1126/science.11.277.620

Van Bavel, C. H. M., Underwood, N., & Swanson, R. W. (1956). Soil moisture measurement by neutron moderation. *Soil Science*, *82*(1), 29–42.

van der Velde, R., Su, Z., van Oevelen, P., Wen, J., Ma, Y., & Salama, M. S. (2012). Soil moisture mapping over the central part of the Tibetan Plateau using a series of ASAR WS images. *Remote Sensing of Environment*, *120*, 175–187. https://doi.org/10.1016/j.rse.2011.05.029

Wang, L., & Qu, J. J. (2009). Satellite remote sensing applications for surface soil moisture monitoring: A review. *Frontiers of Earth Science in China*. https://doi.org/10.1007/s11707-009-0023-7

Williams, P. J. (1967). The nature of freezing soil and its field behaviour, *Publicatio*, 91–119.

Wu, D., Lai, Y., & Zhang, M. (2017). Thermo-hydro-salt-mechanical coupled model for saturated porous media based on crystallization kinetics. *Cold Regions Science and Technology*, *133*, 94–107. https://doi.org/10.1016/j.coldregions.2016.10.012

Xia, Z., & Shufen, S. (2011). The Impact of Soil Freezing/Thawing Processes on Water and Energy Balances. *Advances in Atmospheric Sciences*, *28*(1), 169–177. https://doi.org/10.1007/s00376-010-9206-0.1.Introduction

Xiong, S., Johansson, M. E., Hughes, F. M. R., & Nilsson, C. (2003). Interactive effects of soil moisture, interactive plant canopy, vegetation in a wetland litter and seed addition on plant diversity community. *Journal of Ecology*, *91*(6), 976–986.

Xu, X., Derksen, C., Yueh, S. H., Dunbar, R. S., & Colliander, A. (2016). Freeze/Thaw Detection and Validation Using Aquarius' L-Band Backscattering Data. *IEEE Journal of Selected Topics in Applied Earth Observations and Remote Sensing*, *9*(4), 1370–1381. https://doi.org/10.1109/JSTARS.2016.2519347

Yong, R. (1965). Soil suction effects on partial soil freezing. *Highway Research Rec.*, *68*, 31–42.

Zhang, D., Tang, R., Zhao, W., Tang, B., Wu, H., Shao, K., & Li, Z. L. (2014). Surface soil water content estimation from thermal remote sensing based on the temporal variation of land surface temperature. *Remote Sensing*, *6*(4), 3170–3187. https://doi.org/10.3390/rs6043170

Zheng, D., Van Der Velde, R., Su, Z., Wen, J., Booij, M. J., Hoekstra, A. Y., & Wang, X. (2015). Under-canopy turbulence and root water uptake of a Tibetan meadow ecosystem modeled by Noah-MP. *Water Resources Research*, *51*(7), 5735–5755. https://doi.org/10.1002/2015WR017115

Zhu, X., Shao, M., Zeng, C., Jia, X., Huang, L., Zhang, Y., & Zhu, J. (2016). Application of cosmic-ray neutron sensing to monitor soil water content in an alpine meadow ecosystem on the northern Tibetan Plateau. *Journal of Hydrology*, *536*, 247–254. https://doi.org/10.1016/j.jhydrol.2016.02.038

Zreda, M., Desilets, D., Ferré, T. P. A., & Scott, R. L. (2008). Measuring soil moisture content non-invasively at intermediate spatial scale using cosmic-ray neutrons. *Geophysical Research Letters*, *35*(21), 1–5. https://doi.org/10.1029/2008GL035655

Zreda, M., Shuttleworth, W. J., Zeng, X., Zweck, C., Desilets, D., Franz, T., & Rosolem, R. (2012). COSMOS: The cosmic-ray soil moisture observing system. *Hydrology and Earth System Sciences*, *16*(11), 4079–4099. https://doi.org/10.5194/hess-16-4079-2012

APPENDIX

Appendix A Schedule for the work arrangements in the field work.

Date	Start time	End time	From	To	Distance	Vehicle
Oct. 05	10.05 20:15	10.06 20:20	Amsterdam	Lanzhou	14000km	Airplane
Oct. 06	10.06 20:20	10.06 22:20	LHW	Hotel near LZU	75km	Taxi
	10.06 23:00	10.07 08:00	Hotel near LZU			
Oct. 07	10.07 09:00	10.07 12:00	Collect needed tools in LZU and buy tools not available in the market			
Oct. 08	10.08 09:00	10.08 11:00	Visit staff from LZU			
	10.08 13:00	10.08 21:00	Lanzhou	Maqu	460km	Car
Oct. 09	10.09 06:00	10.09 06:30	Maqu	Experiment site	14km	Car
	10.09 07:00	10.09 19:00	Collect samples and ECH$_2$O observation			
	10.09 19:00	10.09 19:30	Experiment site	Maqu	14km	Car
Oct. 10	10.10 and 10.11 is the same as 10.09					
Oct. 11						
Oct. 12	10.12 08:00	10.12 16:00	Maqu	Lanzhou	460km	Car
	10.12 16:30	10.12 18:00	Weigh the wet samples put the samples in oven			
	10.12 18:00	10.13 14:00	Process the samples in the oven			
Oct. 13	10.13 14:00	10.13 17:00	Weigh the dry samples and rings			
	10.13 18:00	10.13 20:00	Clean up the experiment tools			

Appendix B The soil sampling and theta probe measuring results.

Sample number	Site	Time	Depth	R	W&R	D&R
		UTC+8	cm	g	g	g
1	S1	10:00	0-5	95.60	217.20	167.51
2		10:05	7-12	95.92	227.26	191.50
3		10:10	15-20	99.63	248.33	214.04
4		10:15	25-30	96.19	231.92	207.22
5		10:20	35-40	100.33	276.39	251.52
6	S2	10:30	0-5	99.45	217.46	168.68
7		10:36	7-12	101.79	234.27	191.29
8		10:44	15-20	97.62	264.06	235.47
9		11:52	25-30	NA	NA	NA
10		11:00	35-40	100.71	284.42	260.17
11	S3	12:10	0-5	99.97	210.06	167.64
12		12:15	7-12	98.99	229.39	193.66
13		12:20	15-20	92.83	248.32	216.19
14		12:30	25-30	94.36	242.25	219.36
15		12:40	35-40	97.28	249.32	229.32
16	S4	13:10	0-5	98.95	221.70	167.85
17		13:15	7-12	95.39	227.84	187.68
18		13:20	15-20	99.82	257.83	220.68
19		13:25	25-30	94.56	263.81	229.50
20		13:30	35-40	99.56	286.23	258.78
21	S5	13:50	0-5	86.32	196.44	145.43
22		13:55	7-12	100.76	237.09	197.71
23		14:00	15-20	100.33	256.09	223.82
24		14:05	25-30	101.08	272.03	245.01
25		14:09	35-40	100.60	265.11	245.77
26	S6	14:30	0-5	101.34	218.43	170.69
27		14:32	7-12	95.19	228.15	189.77
28		14:35	15-20	100.10	255.63	222.13
29		14:38	35-40	63.83	171.95	150.53
30		14:40	25-30	68.13	189.92	170.25
31	S7	15:05	0-5	99.39	223.83	178.42
32		15:15	7-12	97.52	231.28	192.19
33		15:25	15-20	94.50	243.25	214.89
34		15:35	25-30	97.50	235.72	216.57
35		13:45	35-40	100.71	260.51	245.23

Soil samples (a) (sample number, site ID, sampling time, depth of sampled soil, weight of sampling ring (R), weight of wet soil and sampling ring (W&R), weight of dry soil and sampling ring (D&R), Not Available (NA)). The soil rings are in the specification of 100 cm^3

Sample Number	Site	Time	Depth	R	W&R	D&R
		UTC+8	cm	g	g	g
36	S8	16:00	0-5	101.43	207.87	162.99
37		16:05	7-12	95.21	230.58	196.46
38		16:10	15-20	96.83	250.85	217.76
39		16:15	25-30	100.92	258.65	227.96
40		16:20	35-40	97.57	251.91	228.98
41	S9	16:30	0-5	102.31	220.85	174.28
42		16:35	7-12	94.54	234.15	192.60
43		16:40	15-20	95.36	256.93	221.58
44		16:43	25-30	96.83	260.51	228.41
45		16:45	35-40	95.52	273.69	245.78
46	S10	17:05	0-5	93.48	216.96	162.54
47		17:10	7-12	101.14	236.97	193.30
48		17:15	15-20	96.27	261.17	225.80
49		17:20	25-30	99.96	264.01	233.69
50		17:25	35-40	94.62	275.93	249.57
51	S11	17:40	0-5	97.22	205.40	161.64
52		17:45	7-12	95.34	230.59	194.91
53		17:50	15-20	100.37	256.93	222.35
54		17:53	25-30	99.29	273.17	246.28
55		17:55	35-40	92.72	267.15	246.17
56	S12	17:58	0-5	97.83	210.53	164.32
57		18:00	7-12	98.95	240.66	200.82
58		18:05	15-20	97.12	236.75	204.47
59		18:07	25-30	97.68	249.46	221.00
60		18:10	35-40	100.08	261.73	239.66
61	S13	18:44	0-5	99.36	216.01	169.77
62		18:50	7-12	94.85	219.21	186.43
63		19:00	15-20	77.65	210.96	181.43
64		19:10	25-30	101.33	246.23	221.35
65		19:17	35-40	96.91	245.12	227.33

Soil samples (b) (sample number, site ID, sampling time, depth of sampled soil, weight of sampling ring (R), weight of wet soil and sampling ring (W&R), weight of dry soil and sampling ring (D&R)). The soil rings are in the specification of 100 cm^3.

Number	Site ID	Time UTC+8	Measuring Results $m^3 m^{-3}$				Mean $m^3 m^{-3}$
1	S1	10:20	0.345				0.3450
2	S2	11:00	0.460				0.4600
3	S3	12:40	0.396	0.404			0.4000
4	S4	13:30	0.503				0.5030
5	S5	14:09	0.464	0.474			0.4690
6	S6	14:40	0.489	0.450			0.4695
7	S7	13:45	0.441	0.446			0.4435
8	S8	16:20	0.393	0.416			0.4045
9	S9	16:45	0.439	0.395			0.4170
10	S10	17:25	0.501	0.488			0.4945
11	S11	17:55	0.440	0.450			0.4450
12	S12	18:10	0.402	0.392			0.3970
13	S13	19:17	0.432	0.402			0.4170
14	θ 1	16:21	0.439	0.452	0.427		0.4393
15	θ 2	18:26	0.435	0.420	0.375		0.4100
16	θ 3	18:28	0.434	0.395	0.422		0.4170
17	θ 4	18:30	0.459	0.457	0.426		0.4473
18	θ 5	18:32	0.463	0.396	0.471		0.4433
19	θ 6	18:34	0.430	0.450	0.421		0.4337
20	θ 7	18:37	0.450	0.467	0.432		0.4497
21	θ 8	18:39	0.460	0.450	0.531	0.410	0.4628

Theta probe measuring result (Measuring number, site ID, sampling time, theta probe measuring results, mean value of theta probe measuring results). The measuring times are may be different at every sites.

Appendix C The example of original CRP data and the meaning of every column.

1601010014.638 - Notepad

File Edit Format View Help

```
//Hydroinnova CRS Probe Filename: 1601010014.638
//****Provide the full data file, with the header information, if support is needed.
//Logger FWVer = 1.944
//Logger SerialNum=14120638
//Probe BootType = 5
//NumberOfNPMs= 2
CRS#1: SerialNum=14110109, FWVer=2338,DeadTime=&H 1f4, RemoteLEDMode=1, NBins=&H  80, U=&H  7d
CRS#2: SerialNum=14070829, FWVer=2338,DeadTime=&H 1f4, RemoteLEDMode=1, NBins=&H  80, U=&H  7d

//Recordperiod = 15 minutes.
//DataSelect=p4p1t1h1t7h7bn1n2e1e2s1s2
//--Data Column Info:
//RecordNum,Date Time(UTC),P4_mb,P1_mb,T1_C,RH1,T_CS215,RH_CS215,Vbat,N1Cts,N2Cts,N1ET_sec,N2ET_sec,N1T_C,N1RH,N2T_C,N2RH,
61, 2016/01/01 00:14:00, 674.44, 675.8,  -9.8,  8.6, -12.7,  8.3, 12.610, 2165, 1140, 901, 901, -4.9,  0.0, -4.1, 0.7
62, 2016/01/01 00:29:00, 674.39, 675.8, -10.4,  8.5, -13.4,  8.2, 12.609, 2126, 1185, 899, 899, -5.3,  0.0, -4.5, 0.7
63, 2016/01/01 00:44:00, 674.65, 676.1, -11.0,  8.3, -14.2,  8.1, 12.606, 2201, 1138, 900, 900, -5.8,  0.0, -5.1, 0.7
64, 2016/01/01 00:59:00, 674.79, 676.2, -11.5,  8.3, -14.5,  8.0, 12.604, 2182, 1103, 900, 900, -6.3,  0.0, -5.6, 0.7
65, 2016/01/01 01:14:00, 674.91, 676.5, -12.0,  8.3, -15.2,  8.1, 12.601, 2235, 1095, 900, 900, -6.7,  0.0, -6.1, 0.7
66, 2016/01/01 01:29:00, 675.05, 676.7, -12.4,  8.3, -15.1,  8.1, 12.599, 2209, 1085, 900, 900, -7.1,  0.0, -6.5, 0.7
67, 2016/01/01 01:44:00, 675.10, 676.7, -12.4,  8.3, -15.0,  7.8, 12.597, 2135, 1164, 900, 900, -7.3,  0.0, -6.5, 0.7
68, 2016/01/01 01:59:00, 675.15, 676.8, -12.6,  8.3, -15.3,  8.0, 12.594, 2117, 1129, 900, 900, -7.6,  0.0, -6.8, 0.7
69, 2016/01/01 02:14:00, 675.31, 676.9, -12.5,  8.4, -14.7,  8.1, 12.601, 2072, 1134, 900, 900, -7.6,  0.0, -6.7, 0.7
70, 2016/01/01 02:29:00, 675.50, 677.1, -12.4,  8.3, -14.9,  7.9, 12.676, 2220, 1192, 900, 900, -7.7,  0.0, -6.7, 0.7
71, 2016/01/01 02:44:00, 675.59, 677.2, -12.2,  8.5, -14.3,  8.3, 12.843, 2113, 1119, 900, 900, -7.7,  0.0, -6.6, 0.7
72, 2016/01/01 02:59:00, 675.76, 677.3, -11.6,  8.7, -13.2,  8.7, 13.325, 2180, 1132, 900, 900, -7.5,  0.0, -6.2, 0.7
73, 2016/01/01 03:14:00, 676.08, 677.5, -10.7,  8.8, -12.3,  8.6, 14.213, 2226, 1084, 900, 900, -7.1,  0.0, -5.5, 0.7
74, 2016/01/01 03:29:00, 676.07, 677.5,  -9.6,  9.0, -11.0,  8.9, 14.963, 2270, 1107, 900, 900, -6.5,  0.0, -4.6, 0.7
75, 2016/01/01 03:44:00, 676.17, 677.4,  -8.1,  9.3,  -9.4,  9.0, 14.963, 2121, 1092, 900, 900, -5.8,  0.0, -3.4, 0.8
76, 2016/01/01 03:59:00, 676.37, 677.4,  -6.7,  9.5,  -8.0,  9.1, 14.963, 2080, 1212, 900, 900, -4.9,  0.0, -2.3, 0.8
77, 2016/01/01 04:14:00, 676.39, 677.3,  -5.3,  9.6,  -6.8,  9.1, 14.961, 2276, 1145, 900, 900, -4.0,  0.0, -1.2, 0.7
78, 2016/01/01 04:29:00, 676.45, 677.4,  -4.2,  9.7,  -5.8,  9.1, 14.924, 2193, 1154, 899, 900, -3.1,  0.0, -0.3, 0.7
81, 2016/01/01 05:14:00, 676.48, 677.2,  -0.4, 13.1,  -2.0, 13.4, 14.408, 2187, 1188, 900, 900, -0.5, -0.0,  2.7, 0.8
```

RecordNum: the record sequence number
Date Time(UTC): the date and time of the recorded data in UTC format
P4_mb: pressure sensor 1 (more reliable, less affected by temperature)
P1_mb: pressure sensor 2 (if available)
T1_C: internal temperature
RH1: internal relative humidity
T_CS215: external temperature (if available)
RH_CS215: external relative humidity (if available)
Vbat: input voltage
N1Cts: moderated detector counts
N2Cts: bare detector counts
N1ET_sec: elapsed time Tube 1
N2ET_sec: elapsed time Tube 2
N1T_C: external temperature Tube 1
N1RH: external relative humidity Tube 1
N2T_C: external temperature Tube 2
N2RH: external relative humidity Tube 2

Appendix D A sample of calculation from neutron counts to TSWC

Raw Data					Correction Factors							Corrected Counts	Final Data		
					Water Vapor Correction				Solar factorCorrection				15 minutes data		
UTC	Moderated Counting Rate	Air Pressure	Air Temperature	Relative Humidity	Barometric Factor	Saturated vapor pressure	Absolute humidity	Water Vapor Factor	Solar Factor	Corrected Solar factor	Total Factor	Corrected Moderated Counting Rate	Local Time	Soil Water Content	+/-
	N_1	P	T	U	f_{bar}	e_w	H	f_{hum}	f_{sol}	f_{sol_cor}	F	$F \cdot N$	UTC +8	q_p	s_{qp}
yyyy-mm-dd h:m	Counts h-1	hPa	°C	%	-	hPa	g m^{-3}	-	-	-	-	Counts hr^{-1}	yyyy-mm-dd h:m	m^3 m^{-3}	m^3 m^{-3}
2016/01/01 00:14:00	2165	674.44	-12.7	8.3	1.01	2.3	0.16	1.00	1.0304	1.0122	1.0258	2221	2016/01/01 08:14:00	0.2614	0.025
2016/01/01 00:29:00	2126	674.39	-13.4	8.2	1.01	2.2	0.15	1.00	1.0304	1.0122	1.0254	2180	2016/01/01 08:29:00	0.2860	0.028
2016/01/01 00:44:00	2201	674.65	-14.2	8.1	1.01	2.0	0.14	1.00	1.0304	1.0122	1.0274	2261	2016/01/01 08:44:00	0.2396	0.023
2016/01/01 00:59:00	2182	674.79	-14.5	8.0	1.02	2.0	0.13	1.00	1.0304	1.0122	1.0285	2244	2016/01/01 08:59:00	0.2486	0.024
2016/01/01 01:14:00	2235	674.91	-15.2	8.1	1.02	1.9	0.13	1.00	1.0314	1.0126	1.0298	2302	2016/01/01 09:14:00	0.2199	0.021
2016/01/01 01:29:00	2209	675.05	-15.1	8.1	1.02	1.9	0.13	1.00	1.0314	1.0126	1.0309	2277	2016/01/01 09:29:00	0.2315	0.022
2016/01/01 01:44:00	2135	675.10	-15.0	7.8	1.02	1.9	0.13	1.00	1.0314	1.0126	1.0313	2202	2016/01/01 09:44:00	0.2726	0.027
2016/01/01 01:59:00	2117	675.15	-15.3	8.0	1.02	1.9	0.13	1.00	1.0314	1.0126	1.0317	2184	2016/01/01 09:59:00	0.2834	0.028
2016/01/01 02:14:00	2072	675.31	-14.7	8.1	1.02	2.0	0.13	1.00	1.0370	1.0148	1.0353	2145	2016/01/01 10:14:00	0.3093	0.031
2016/01/01 02:29:00	2220	675.50	-14.9	7.9	1.02	1.9	0.13	1.00	1.0370	1.0148	1.0368	2302	2016/01/01 10:29:00	0.2199	0.021
2016/01/01 02:44:00	2113	675.59	-14.3	8.3	1.02	2.0	0.14	1.00	1.0370	1.0148	1.0376	2192	2016/01/01 10:44:00	0.2783	0.027
2016/01/01 02:59:00	2180	675.76	-13.2	8.7	1.02	2.2	0.16	1.00	1.0370	1.0148	1.0390	2265	2016/01/01 10:59:00	0.2377	0.023
2016/01/01 03:14:00	2226	676.08	-12.3	8.6	1.03	2.4	0.17	1.00	1.0337	1.0135	1.0403	2316	2016/01/01 11:14:00	0.2134	0.021
2016/01/01 03:29:00	2270	676.07	-11.0	8.9	1.03	2.7	0.20	1.00	1.0337	1.0135	1.0404	2362	2016/01/01 11:29:00	0.1938	0.019
2016/01/01 03:44:00	2121	676.17	-9.4	9.0	1.03	3.0	0.22	1.00	1.0337	1.0135	1.0413	2209	2016/01/01 11:44:00	0.2685	0.026
2016/01/01 03:59:00	2080	676.37	-8.0	9.1	1.03	3.4	0.25	1.00	1.0337	1.0135	1.0431	2170	2016/01/01 11:59:00	0.2927	0.029
2016/01/01 04:14:00	2276	676.39	-6.8	9.1	1.03	3.7	0.27	1.00	1.0284	1.0114	1.0412	2370	2016/01/01 12:14:00	0.1906	0.018
2016/01/01 04:29:00	2193	676.45	-5.8	9.1	1.03	4.0	0.29	1.00	1.0284	1.0114	1.0418	2285	2016/01/01 12:29:00	0.2280	0.022
2016/01/01 05:14:00	2187	676.48	-2.0	13.4	1.03	5.3	0.57	1.00	1.0221	1.0088	1.0409	2277	2016/01/01 13:14:00	0.2319	0.022
2016/01/01 05:31:16	1974	676.46	1.8	15.6	1.03	7.0	0.86	1.00	1.0221	1.0088	1.0424	2058	2016/01/01 13:31:16	0.3794	0.040
2016/01/01 05:45:00	1974	676.33	1.3	12.6	1.03	6.7	0.67	1.00	1.0221	1.0088	1.0403	2054	2016/01/01 13:45:00	0.3832	0.040
2016/01/01 06:00:00	2093	676.30	1.7	11.5	1.03	6.9	0.63	1.00	1.0198	1.0079	1.0389	2174	2016/01/01 14:00:00	0.2896	0.029
2016/01/01 06:15:00	2098	676.03	2.7	12.7	1.03	7.4	0.74	1.00	1.0198	1.0079	1.0374	2176	2016/01/01 14:15:00	0.2883	0.028
2016/01/01 06:30:00	2143	676.00	2.8	11.2	1.02	7.5	0.66	1.00	1.0198	1.0079	1.0367	2222	2016/01/01 14:30:00	0.2610	0.025
2016/01/01 06:45:00	2160	675.63	3.3	10.7	1.02	7.7	0.65	1.00	1.0198	1.0079	1.0337	2233	2016/01/01 14:45:00	0.2548	0.025
2016/01/01 07:00:00	2193	675.08	3.8	10.4	1.02	8.0	0.65	1.00	1.0145	1.0058	1.0272	2253	2016/01/01 15:00:00	0.2441	0.024
2016/01/01 07:15:00	2259	675.05	4.3	10.2	1.02	8.3	0.66	1.00	1.0145	1.0058	1.0270	2320	2016/01/01 15:15:00	0.2116	0.020
2016/01/01 07:30:00	2216	674.85	4.4	10.0	1.02	8.4	0.65	1.00	1.0145	1.0058	1.0253	2272	2016/01/01 15:30:00	0.2341	0.023
2016/01/01 07:45:00	2234	674.46	4.2	9.8	1.01	8.2	0.63	1.00	1.0145	1.0058	1.0222	2283	2016/01/01 15:45:00	0.2285	0.022
2016/01/01 08:00:00	2224	674.18	3.8	9.7	1.01	8.0	0.61	1.00	1.0106	1.0042	1.0182	2265	2016/01/01 16:00:00	0.2379	0.023
2016/01/01 08:15:00	2243	673.98	3.8	9.6	1.01	8.0	0.60	1.00	1.0106	1.0042	1.0166	2280	2016/01/01 16:15:00	0.2301	0.022
2016/01/01 08:30:00	2267	673.96	4.0	9.5	1.01	8.1	0.60	1.00	1.0106	1.0042	1.0165	2304	2016/01/01 16:30:00	0.2186	0.021
2016/01/01 08:45:00	2293	673.76	4.4	9.4	1.01	8.4	0.61	1.00	1.0106	1.0042	1.0150	2327	2016/01/01 16:45:00	0.2083	0.020

Appendix E The smoothed results of soil water content derived from neutron counts compared with soil water content from point measurement with different time windows.